BIOCHEMISTRY
including biophysical chemistry & molecular biology

Article

pubs.acs.org/biochemistry

Isomerase-Catalyzed Binding of Interleukin-1 Receptor-Associated Kinase 1 to the EVH1 Domain of Vasodilator-Stimulated Phosphoprotein

Alexander I. Greenwood, Jeahoo Kwon, and Linda K. Nicholson*

Department of Molecular Biology and Genetics, Cornell University, Ithaca, New York 14853, United States

Supporting Information

ABSTRACT: Interleukin-1 receptor-associated kinase 1 (IRAK1) is a crucial signaling kinase in the immune system, involved in Toll-like receptor signaling. Vasodilator-stimulated phosphoprotein (VASP) is a central player in cell migration that regulates actin polymerization and connects signaling events to cytoskeletal remodeling. A VASP−IRAK1 interaction is thought to be important in controlling macrophage migration in response to protein kinase C-ε activation. We show that the monomeric VASP EVH1 domain directly binds to the $_{168}$WPPPP$_{172}$ motif in the IRAK1 undefined domain (IRAK1-UD) with moderate affinity (K_D^{App} = 203 ± 3 μM). We further show that this motif adopts distinct *cis* and *trans* isomers for the Trp168−Pro169 peptide bond with nearly equal populations, and that binding to the VASP EVH1 domain is specific for the *trans* isomer, coupling binding to isomerization. Nuclear magnetic resonance line shape analysis and tryptophan fluorescence experiments reveal the complete kinetics and thermodynamics of the binding reaction, showing diffusion-limited binding to the *trans* isomer followed by slow, isomerization-dependent binding. We further demonstrate that the peptidyl-prolyl isomerase cyclophilin A (CypA) catalyzes isomerization of the Trp168−Pro169 peptide bond and accelerates binding of the IRAK1-UD to the VASP EVH1 domain. We propose that binding of IRAK1 to tetrameric VASP is regulated by avidity through the assembly of IRAK1 onto receptor-anchored signaling complexes and that an isomerase such as CypA may modulate IRAK1 signaling *in vivo*. These studies demonstrate a direct interaction between IRAK1 and VASP and suggest a potential mechanism for how this interaction might be regulated by both assembly of IRAK1 onto an activated signaling complex and PPIase enzymes.

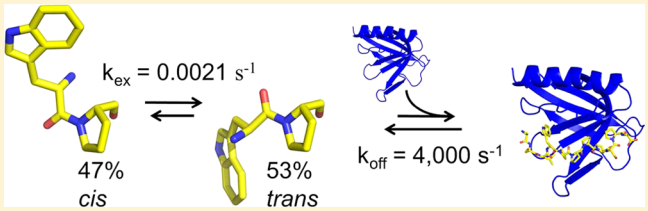

Toll-like receptors (TLRs) provide the first line of defense against viral, bacterial, and fungal invaders.[1] These receptors recognize specific pathogen-associated molecular patterns that are not normally present in the host, such as flagellin, double-stranded RNA, and lipopolysaccharides.[2−4] To date, at least 10 distinct human TLRs have been identified, some of which reside in the plasma membrane to detect extracellular pathogen-associated ligands, while others are localized to intracellular compartments where they detect endocytosed pathogen-associated ligands.[1,5] Activation of TLRs triggers signaling cascades that upregulate the expression of type I interferons and proinflammatory cytokines to orchestrate innate and adaptive immunity. Such cytokines include interleukin-1 β and the related IL-18, which are recognized by the interleukin-1 receptor (IL-1R) family of receptors. TLRs and IL-1Rs share a homologous cytoplasmic Toll/IL-1 receptor (TIR) domain and are therefore classified together as members of the Toll/IL-1 family of receptors.[6]

While Toll/IL-1 receptors and their ligands are diverse, the signaling pathways of several of these receptors share specific components, such as the adaptor protein MyD88 and the interleukin-1-receptor associated kinase (IRAK) family of proteins (IRAK1, IRAK2, IRAKM, and IRAK4).[6,7] Each IRAK family member contains two folded domains (a death domain and a serine/threonine kinase domain) separated by a linker region that is unique to each family member, and a C-terminal region. The death domain is an oligomerization module that mediates interactions with activated signaling complexes,[8,9] while the kinase domains of all but IRAKM (whose kinase domain is inactive) participate in phosphorylation-mediated signaling events.[10−14] IRAK1 plays a key role in innate immunity signaling through both TLRs and IL-1Rs, as it assembles via its death domain onto the signaling complex known as the Myddosome.[15,16] Although key signaling functions are attributed to the kinase activity of IRAK1,[11,17−19] important IRAK1 signaling interactions are thought to be mediated by its undefined domain (Figure 1A), as well.[20−24]

The IRAK1 undefined domain (IRAK1-UD) is a 95-residue proline-rich region containing 27 Pro residues. To date, three proteins have been implicated as specific binding partners for this domain, namely, Pin1,[20] NEMO,[21] and Pellino.[22−24] Additionally, the vasodilator-stimulated phosphoprotein (VASP), a cytoskeletal rearrangement protein, has recently been shown to co-immunoprecipitate and functionally interact with IRAK1 in the regulation of macrophage migration.[25]

Received: January 8, 2014
Revised: April 13, 2014
Published: May 12, 2014

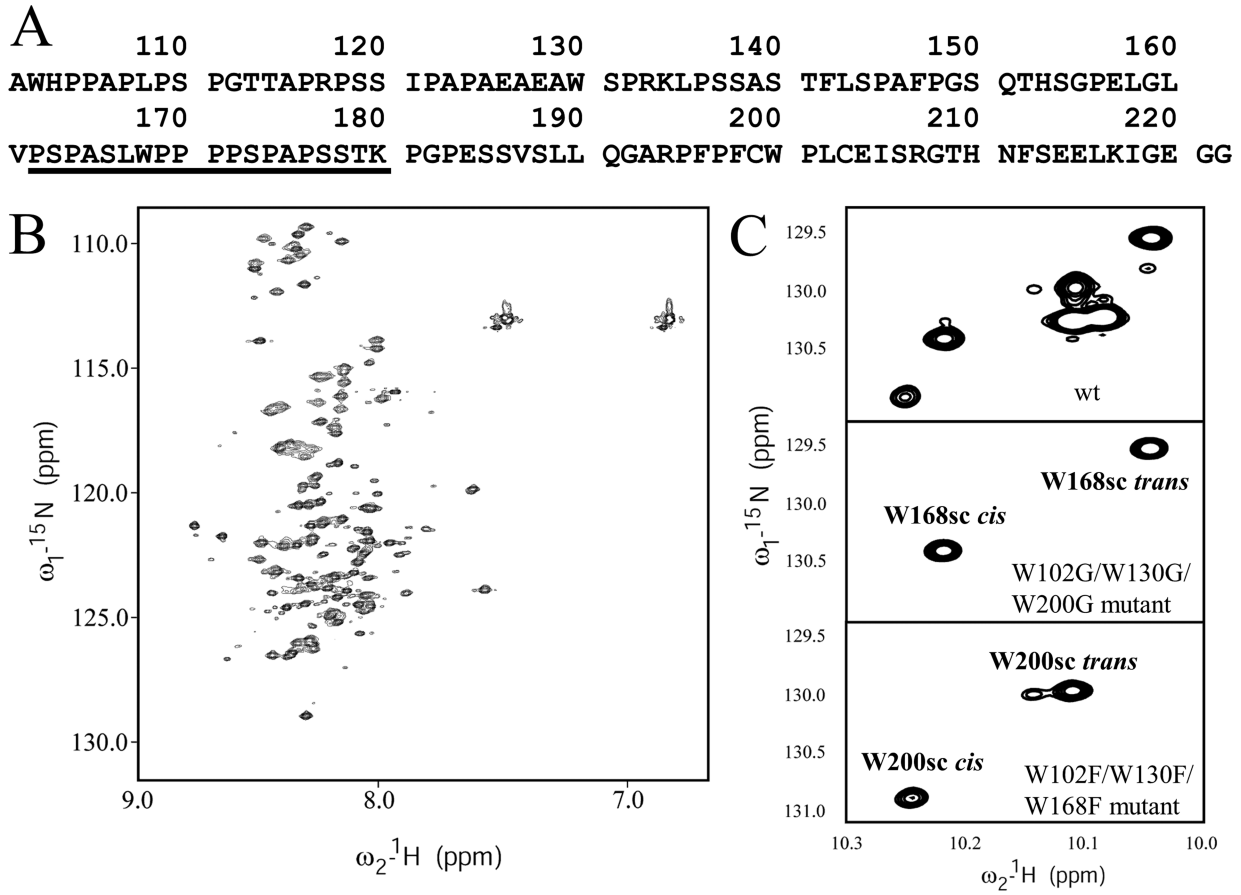

Figure 1. Conformational heterogeneity in the undefined domain of IRAK1. (A) Sequence of the IRAK1-UD construct used (IRAK1 residues 101−222). The sequence of IRAK1$^{162-180}$ is underlined. The backbone NH region of the ^{15}N−^{1}H HSQC spectrum of the IRAK1-UD (B) shows a very narrow chemical shift dispersion, indicating that the UD does not adopt a stable fold. The tryptophan side chain (sc) indole peaks, located downfield (C), display six peaks for the four tryptophans in the sequence (top). The two W−P motifs in this sequence, W168 and W200 (middle and bottom, respectively), were identified by mutating the other tryptophans (using the W102G/W130G/W200G and W102F/W130F/W168F IRAK1-UD mutants, respectively), and the *cis* and *trans* isomers of each are labeled.

Cellular localization of VASP is mediated by an N-terminal Ena/VASP homology 1 (EVH1) domain, a binding module that recognizes the proline-rich motif (W/F)PxφP,[26−28] where x is any amino acid, φ is an aliphatic residue, and x and φ are frequently proline. This motif is present in the focal adhesion proteins zyxin and vinculin and the *Listeria monocytogenes* surface protein ActA, as well as in IRAK1.[25,29] The interaction between VASP and IRAK1 is predicted to be mediated by the EVH1 domain of VASP, because the IRAK1-UD contains an EVH1 binding motif ($_{168}$WPPPP$_{172}$) and mutation of IRAK1 in this site (L167A and W168A) prevents co-immunoprecipitation of IRAK1 and VASP.[25] However, because co-immunoprecipitation can be mediated by additional factors, a direct interaction between the VASP EVH1 domain and the IRAK1-UD was not demonstrated.

VASP is a founding member of the Ena/VASP family.[30,31] Ena/VASP proteins are important actin-binding proteins that regulate the actin cytoskeleton by increasing actin filament length, and tend to localize at sites with high actin cytoskeleton dynamics such as filapodial tips and the periphery and ruffles of lamellae.[32] Ena/VASP proteins also participate in the concerted regulation of actin polymerization in the adherens junctions[33,34] and focal adhesions,[35] where the cytoskeleton must dynamically assemble and disassemble in migrating cells.[36] The localization of Ena/VASP proteins can occur in response to receptor-mediated signals that trigger cytoskeletal remodeling, and this regulated spatial targeting is a critical aspect of directing cytoskeletal dynamics to the right place at the right time.[30] The central role of Ena/VASP proteins in cellular processes involving cytoskeletal remodeling, such as axon guidance,[37] migration,[30,38] and cell−cell interaction,[33,39] warrants detailed characterization of interactions that are implicated in localizing them to specific sites, such as the IRAK1−VASP interaction.[25]

Here we report nuclear magnetic resonance (NMR) and fluorescence studies that quantify the interaction between the IRAK1-UD and the VASP EVH1 domain. These studies demonstrate the direct interaction between the $_{168}$WPPPP$_{172}$ motif of IRAK1 and the canonical EVH1 binding surface, measure the affinity of this 1:1 interaction, and provide the kinetic rates for both fast binding and slow isomerization. NMR titration data from the [^{15}N]IRAK1-UD perspective reveal the specificity of this interaction for the *trans* isomer of the W_{168}−P_{169} peptide bond, while titration data from the [^{15}N]VASP-EVH1 perspective yield the affinity and the microscopic rate constants for the binding reaction. Strikingly, at equilibrium, the W_{168}−P_{169} peptide bond is 47% *cis* and 53% *trans*, with nearly half of the protein in the *cis* conformation, incapable of binding to the VASP EVH1 domain. Application of the ^{15}N ZZ-exchange NMR experiment, which utilizes the transfer of heteronuclear longitudinal spin magnetization to measure

dx.doi.org/10.1021/bi500031e | *Biochemistry* 2014, 53, 3593−3607

exchange between different chemical environments, shows that the peptidyl-prolyl isomerase enzyme cyclophilin A (CypA) catalyzes isomerization of the $W_{168}-P_{169}$ peptide bond. Fluorescence time course experiments yield the rate of uncatalyzed *cis*–*trans* isomerization of the $W_{168}-P_{169}$ peptide bond and show that CypA effectively catalyzes binding. These studies suggest that this relatively weak 1:1 interaction (K_D^{App} = 203 ± 3 μM) could act as a molecular switch, possibly regulated by avidity when tetrameric VASP encounters oligomerized IRAK1 on an activated TLR or IL-1R signaling complex, with the rate of achievement of full avidity enhancement modulated by isomerase activity (e.g., by CypA). These results provide an intriguing link between innate immunity signaling and cytoskeletal rearrangement and novel insights into the coupled roles of oligomerization-triggered avidity enhancement and prolyl isomerization in the regulation of this link.

MATERIALS AND METHODS

Protein and Peptide Preparation. All proteins were expressed as N-terminal six-His-tagged fusion proteins in BL21-DE3 *Escherichia coli* cells. The human IRAK1-UD (IRAK1 residues 101–222) was encoded in a pET vector (kanamycin resistance) with a TEV protease cleavage site between the six-His tag and the protein. The human VASP EVH1 domain (VASP residues 2–115) was encoded in a pMW172 vector (ampicillin resistance, a gift from M. Way, London Research Institute, London, U.K.) with a 3Cpro protease cleavage site between the six-His tag and protein as described previously.[40] Human CypA (full-length) was encoded in a pTFT74 vector (ampicillin resistance, gift from C. Kalodimos, Rutgers University, Piscataway, NJ) without a cleavage site as described previously.[41] Cells were grown in 1 L of M9 medium with 19 mM $^{15}NH_4Cl$ (or natural abundance NH_4Cl to produce unlabeled protein) and an antibiotic at 37 °C until they reached an OD_{600} of ∼0.8. Protein expression was then induced with 1 mM IPTG for ∼4 h at 37 °C (IRAK1-UD) or ∼16 h at 18 °C (VASP EVH1 domain and CypA), after which cells were harvested and resuspended in 20 mL of wash buffer [50 mM NaH_2PO_4, 300 mM NaCl, 20 mM imidazole, and 0.1 mM TCEP (pH 8.0)] with 100 μL of protease inhibitor cocktail and 1 mM TCEP added. Cells were lysed by freezing and thawing them, adding 20 mg of lysozyme, and sonicating them on ice for 10 cycles. Cell debris was removed by centrifugation at 23000*g* followed by filtering the supernatant with a 0.8 μm syringe filter. The filtrate was passed through a nickel-NTA column that was then washed with 20 bed volumes of wash buffer. Protein was eluted with 10 mL of elution buffer [50 mM Na_2HPO_4, 300 mM KCl, and 100 mM imidazole (pH 8.0)] and dialyzed into cleavage buffer [50 mM Tris-HCl and 1 mM TCEP (pH 8.0)] or NMR buffer [20 mM KH_2PO_4, 50 mM KCl, and 1 mM TCEP (pH 6.7)] in the case of CypA. After dialysis, recombinant His-tagged 3C protease or TEV protease was added to the protein sample and the cleavage reaction was performed overnight at 4 °C. The His tag and His-tagged protease were then removed by passing the cleavage reaction back through a nickel-NTA column. The flow-through was dialyzed in NMR buffer and concentrated with 5000 molecular weight cutoff centrifugal concentrators as necessary. NMR samples also contained 5 mM NaN_3 and 7% D_2O. The NMR sample in the ^{15}N ZZ-exchange experiment had 10 mM TCEP to prevent oxidation of the especially concentrated sample. The protein concentration was measured by UV absorbance using the theoretical extinction coefficients at 280 nm of 22000 cm^{-1} M^{-1} for the wild-type IRAK1-UD, 21000 cm^{-1} M^{-1} for the VASP EVH1 domain, and 8500 cm^{-1} M^{-1} for CypA. Plasmids encoding the IRAK1-UD mutants W102G/W130G/W200G and W102F/W130F/W168F were generated by three sequential rounds of site-directed mutagenesis using the QuikChange protocol (Stratagene); mutant IRAK1-UD proteins were produced as described above, and protein concentrations were determined using the adjusted theoretical extinction coefficient (5500 cm^{-1} M^{-1}).

A synthetic peptide encompassing IRAK1 residues $P_{162}-K_{180}$ [$IRAK1^{162-180}$ (Figure 1A)] was purchased and received as a lyophilized powder (Tufts Core Facility, Boston, MA). Likewise, a peptide encompassing ActA residues 333–344 ($ActA^{333-344}$) was purchased from Genscript (Piscataway, NJ). Peptides were dissolved in NMR buffer, and concentrations were determined by UV absorbance, using theoretical extinction coefficients of 5500 cm^{-1} M^{-1} at 280 nm for $IRAK1^{162-180}$ and 390 cm^{-1} M^{-1} at 257 nm for $ActA^{333-344}$. The sample pH was adjusted using NaOH and HCl before use.

NMR Data Collection and Processing. All NMR experiments were performed on a Varian Inova 600 MHz spectrometer equipped with a {H, C, N} *Z*-axis gradient probe. Unless otherwise stated, NMR experiments were performed at 25 °C. All NMR spectra were processed and analyzed with nmrPipe,[42] nmrDraw,[42] and Sparky.[43] Either an exponential or phase-shifted sine bell window function was applied to free induction decays prior to Fourier transformation. The Sparky peak detection function was used to measure peak positions, volumes, and heights.

NMR Titration Experiments. Altogether, four titration experiments were conducted. Three titrations of the [^{15}N]EVH1 domain (with the unlabeled IRAK1-UD, $IRAK1^{162-180}$, and $ActA^{333-344}$) were performed, as well as a titration of the [^{15}N]IRAK1-UD with the unlabeled EVH1 domain. In each titration, the most saturated sample was prepared first and the subsequent titration samples were prepared by mixing a portion of the previous sample with a stock of equal concentration of the labeled protein, thus keeping the concentration of labeled protein constant while varying the titrant concentration. All titrations were performed in NMR buffer as follows. In the titration of the [^{15}N]EVH1 domain with the IRAK1-UD, the concentration of EVH1 was held at 0.51 mM and the IRAK1-UD concentrations were 0, 0.07, 0.11, 0.17, 0.25, 0.38, 0.56, 0.84, and 1.27 mM. In the titration of the [^{15}N]EVH1 domain with $IRAK1^{162-180}$, the concentration of the [^{15}N]EVH1 domain was held between 0.35 and 0.38 mM and the peptide concentrations were 0, 0.03, 0.06, 0.12, 0.24, 0.48, 0.95, 1.9, and 3.8 mM. In the titration of the [^{15}N]EVH1 domain with $ActA^{333-344}$, the concentration of the [^{15}N]EVH1 domain was held at 0.37 mM and the peptide concentrations were 0, 0.04, 0.08, 0.15, 0.30, 0.61, 1.21, 2.43, and 4.86 mM. In the titration of the [^{15}N]IRAK1-UD with the EVH1 domain, the concentration of the [^{15}N]IRAK1-UD was held at 0.34 mM and the EVH1 concentrations were 0, 0.18, 0.35, and 0.70 mM. For each titration condition, a $^{15}N-^{1}H$ fast HSQC[44] spectrum was recorded with a spectral width of 8 kHz in the proton dimension (total of 2048 complex data points) and 1.7 kHz ([^{15}N]IRAK1-UD perspective titration and [^{15}N]EVH1 perspective IRAK1-UD titration) or 1.8 kHz ([^{15}N]EVH1 domain peptide titrations) in the nitrogen dimension (total of 256 complex data points).

Quantification of Binding and NMR Line Shape Analysis. The peak trajectories of resolved residues in NMR

dx.doi.org/10.1021/bi500031e | *Biochemistry* 2014, 53, 3593–3607

titrations were used to determine binding constants. For a given peak, the change in chemical shift between the apo spectrum and a titration point spectrum for the proton and nitrogen dimensions, $\Delta\delta_H$ and $\Delta\delta_N$, was fit as a function of the apparent dissociation constant, K_D^{App}, and the protein and peptide molar concentrations. For given total concentrations of the EVH1 domain, [EVH1^{tot}], and IRAK1, [IRAK1^{tot}], the concentration of the bound complex, [EVH1:IRAK1], is given by

$$[\text{EVH1:IRAK1}] = \frac{1}{2}\{K_D^{App} + [\text{EVH1}^{tot}] + [\text{IRAK1}^{tot}] - ((K_D^{App} + [\text{EVH1}^{tot}] + [\text{IRAK1}^{tot}])^2 - 4[\text{EVH1}^{tot}]\cdot[\text{IRAK1}^{tot}])^{1/2}\} \quad (1)$$

Using chemical shift changes of [^{15}N]EVH1 domain peaks, K_D^{App} was determined from the titrations of the [^{15}N]EVH1 domain with the IRAK1-UD and IRAK1$^{162-180}$ using the equation

$$[\text{EVH1:IRAK1}] = \frac{\Delta\delta_i}{\Delta\delta_i^{max}}[\text{EVH1}^{tot}] \quad (2)$$

where i is H or N and $\Delta\delta^{max}$ is the chemical shift difference between the free and bound forms (a fitted parameter). To account for inaccuracies in the calculation of the extinction coefficient, the concentrations of peptide in the ActA$^{333-344}$ titration were scaled by a fitted correction factor, L_{corr}, using the equation $[\text{ActA}^{333-344}]_{corrected} = [\text{ActA}^{333-344}]_{measured}L_{corr}$. This was warranted given the sharp binding curves, which were very sensitive to stoichiometry. For each titration set, the reported K_D^{App} value and its uncertainty were determined by fitting each of 21 ^{1}H and 21 ^{15}N chemical shift data sets independently and taking the mean and standard error of the resulting fitted values. Values of K_D^{trans} were obtained using eq 5, and uncertainties were obtained by propagating the uncertainties in K_D^{App} and K_{isom}. Fits were performed by least-squares minimization using the Solver function in Microsoft Excel.

Line shape analysis of the [^{15}N]EVH1 domain peptide titrations was conducted as described previously,[45] using the *BiophysicsLab* Matlab package (currently, Integrative Data Analysis Platform, IDAP;[46] http://kovrigin.chem.mu.edu/IDAP/). Line shapes were extracted as one-dimensional (1D) slices in each dimension (^{1}H and ^{15}N) using the *BiophysicsLab* Sparky extension. To eliminate any titration-dependent variation in signal intensity, the area under each peak slice was normalized. The software calculates the populations of the free and bound EVH1 domain using eq 1 and simulates line shape data using the two-state solution to the Bloch–McConnell equations.[47,48] The dissociation constant, K_D^{App}, apo chemical shift, ω^{Apo}, and line width of the apo state, $R_{2,0}^{Apo}$, previously determined by peak positions and the spectrum of apo [^{15}N]EVH1 domain were constrained, while the dissociation rate, k_{off}, bound chemical shift, ω^{Bound}, and line width of the bound state, $R_{2,0}^{Bound}$, were determined by least-squares fitting. We report the average and standard error of the fitted parameters k_{off} and k_{on} from individual fits of four line shape data sets. A global fit that yielded statistically equivalent values of these parameters was also performed.

Modeling the IRAK1:EVH1 Complex. The model of the VASP EVH1 domain bound to IRAK1$^{162-180}$ was built using a solution structure of the VASP EVH1 domain [Protein Data Bank (PDB) entry 1EGX[28]] and a crystal structure of the complex between the Mena EVH1 domain and an ActA-derived peptide (PDB entry 1EVH[49]) with an FPPPPT sequence. The Mena and VASP EVH1 structures were overlaid using the "magic fit" function in Swiss-Pdb viewer.[50] The IRAK1 sequence of residues A165–A175 was introduced into the binding site by changing the ActA peptide (chain B) in the complex crystal structure to the IRAK1 sequence using the "mutate" and "add residue" functions in Swiss-Pdb viewer. The torsion angles of W168 in the IRAK1 peptide were adjusted to align the indole ring with the phenylalanine side chain in the ActA peptide sequence, and the torsion angles of R83 in the EVH1 domain were adjusted slightly to accommodate the bound peptide. Energy minimization was performed using the GROMOS96 implementation within Swiss-Pdb viewer.

Demonstration of Isomerization by ^{15}N ZZ-Exchange Spectroscopy. ^{15}N ZZ-exchange spectroscopy[51] was performed on a 0.8 mM [^{15}N]IRAK1-UD sample, with or without 8 μM CypA in NMR buffer. Mixing times were 0, 0.01101, 0.02202, 0.03303, 0.04404, 0.05505, 0.082575, and 0.1101 s. For each spectrum, a spectral width of 8 kHz (total of 2048 complex data points) was used in the proton dimension, and 1.7 kHz (total of 256 data points) in the nitrogen dimension, with 40 transients per free induction decay and a recycle delay of 1.0 s. To assist in identifying cross peaks, the spectra with non-zero mixing times were added together using the NMRPipe command addNMR. To determine the rate of W168–P169 isomerization, peak heights for autopeaks and cross peaks corresponding to the side chain of W168 were obtained using Sparky. The heights of these four peaks as a function of mixing time were fit to the two-state solution of the Bloch–McConnell equations[47,48] by least-squares minimization with Microsoft Excel (Solver function). The ^{15}N longitudinal relaxation constants for the *cis* and *trans* isomers, $R_{1,0}^{trans}$ and $R_{1,0}^{cis}$ (determined by running the ^{15}N ZZ-exchange experiment without CypA), and the ratio of *trans* to *cis* isomer, K_{isom} (determined from peak volumes corresponding to the *cis* and *trans* isomers of the W_{168}–P_{169} peptide bond), were treated as fixed parameters. Fitted parameters included the initial intensities of autopeaks, $I_{TT,0}$ and $I_{CC,0}$, and the exchange rate of isomerization, k_{ex}. The mixing time dependencies of all four peaks were fit simultaneously. Monte Carlo analysis was performed as described previously,[52] varying the values of $R_{1,0}^{trans}$, $R_{1,0}^{cis}$, and K_{isom} as well as the peak intensity data within their uncertainties to determine the uncertainty in the value of k_{ex}.

Tryptophan Fluorescence Experiments. All tryptophan fluorescence experiments were conducted using an F-7000 fluorescence spectrophotometer (Hitachi High Technologies America, Schaumburg, IL). In mixing experiments, 2 mL of 100 μM (IRAK1$^{162-180}$ experiment) or 77 μM (ActA$^{333-344}$ experiment) EVH1 domain, with or without 62 nM CypA, was equilibrated in a quartz cuvette and gently stirred while the temperature was held at 25 °C. The peptide was then added from a concentrated stock into the cuvette for a final concentration of 53 μM (IRAK1$^{162-180}$ experiment) or 50 μM (ActA$^{333-344}$ experiment), and a time course was recorded (2 s interval, 40 min, or 0.5 s interval, 20 min). The fluorescence signal was measured by excitation at 294 nm and collection at 360 nm (2.5 nm bandpass for excitation, 20 nm bandpass for emission) for the IRAK1$^{162-180}$ experiment and excitation at 290 nm and collection at 334 nm (2.5 nm bandpass for excitation, 20 nm bandpass for emission) for the ActA$^{333-344}$ experiment. In the dilution experiments, 4 μL of an equilibrated stock containing 1 mM EVH1 domain and 1 mM IRAK1$^{162-180}$ was diluted into 2 mL of NMR buffer (or NMR

buffer with a catalytic quantity of CypA) in a stirred and temperature-controlled (20, 25, and 30 °C) quartz cuvette. A time course was then recorded (1 or 0.5 s interval, 15−50 min). The fluorescence signal was measured by excitation at 280 nm and collection at 360 nm (1.0 nm bandpass for excitation, 20 nm bandpass for emission). Fluorescence data were fit following subtraction of a baseline, which was determined from taking data of the EVH1 domain prior to adding peptide or, for the dilution experiments, using the data from long after the exponential signal had stabilized. Data were fit to the exponential function

$$I(t) = I_{\text{final}} + (I_0 - I_{\text{final}})e^{-tk_{\text{obs}}} \quad (3)$$

where I_{final} and I_0 are the equilibrium and initial fluorescence intensities, respectively, and k_{obs} is the rate constant given by[45,53,54]

$$k_{\text{obs}} + k_{\text{CT}} + k_{\text{TC}}/\left(1 + \frac{[\text{EVH1}^{\text{free}}]}{K_{\text{D}}^{\text{App}}}\right) \quad (4)$$

where k_{CT} and k_{TC} are the *cis*-to-*trans* and *trans*-to-*cis* rates of isomerization, respectively. Rates k_{CT} and k_{TC} reflect the intrinsic isomerization rates when the experiment is performed in the absence of CypA but increase linearly with CypA concentration. Equation 4 is an approximation that requires that the kinetics of binding be fast compared to the kinetics of isomerization, and that $[\text{EVH1}^{\text{free}}]$ be treated as a time-independent parameter. In the dilution experiment, $[\text{EVH1}^{\text{free}}]/K_{\text{D}}^{\text{App}}$ approximates to 0 and the equation reduces to $k_{\text{obs}} = k_{\text{CT}} + k_{\text{TC}} = k_{\text{CT}}(1 + 1/K_{\text{isom}})$.

To measure the affinity of binding of the EVH1 domain to $\text{ActA}^{333-344}$ using tryptophan fluorescence, 50 μM EVH1 domain with 1 μM CypA was incubated in the quartz cuvette at 25 °C and $\text{ActA}^{333-344}$ was titrated in 7 μM increments. Data were collected as a time course to monitor the stability of the signal. For each titration point, a time course was collected (10 s, 0.1 s interval) and the average fluorescence signal at each peptide concentration was fit to a standard bimolecular binding curve in analogy to eqs 1 and 2. As in the NMR titration, the peptide concentration was scaled by a fitted correction factor to account for inaccuracies in the extinction coefficient calculation. All fitting of fluorescence data was performed by least-squares minimization using the Solver function in Microsoft Excel.

RESULTS

The Undefined Domain of IRAK1 Is Conformationally Heterogeneous. As a first step in the characterization of the IRAK1/VASP interaction, the ^{15}N-labeled human IRAK1-UD [residues 101−222 (Figure 1A)] was examined by two-dimensional NMR spectroscopy. The [^{15}N]IRAK1-UD yields a ^{15}N−^{1}H HSQC spectrum with very narrow peak dispersion, characteristic of a disordered polypeptide (Figure 1B). Furthermore, it displays a number of minor peaks at the low contour level, which, given the 27 proline residues in this sequence, could be attributed to the *cis* isomers of the various X−Pro peptide bonds (demonstrated below). Because *cis*−*trans* isomerization is a slow process with an exchange time constant (τ) on the order of minutes in the absence of isomerase activity,[55] an equilibrium between *cis* and *trans* isomers generally results in two distinct NMR peaks for residues whose chemical environment differs for the two isomers. The four Trp indole NHs in this sequence give rise to six peaks (Figure 1C), with the two W−P motifs (W_{168}−P_{169} and W_{200}−P_{201}) each giving rise to two peaks corresponding to their comparable *cis* and *trans* populations. Unique resonance assignments of the W_{168} and W_{200} indole NH peaks were obtained via mutagenesis (Figure 1C). On the basis of peak volumes, the equilibrium *cis* and *trans* populations of the W_{168}−P_{169} peptide bond are nearly equal (47% *cis* and 53% *trans* by ^{15}N−^{1}H HSQC, ^{1}H TOCSY, and 1D spectra), yielding an equilibrium constant (K_{isom}) of 1.15 ± 0.08, where the uncertainty is estimated from the variability between different pairs of peaks and between different spectra. Similarly, the population of the W_{200}−P_{201} peptide bonds is 35% *cis* and 65% *trans*. This is consistent with the intrinsic tendency of the bulky tryptophan side chain to induce a large *cis* population when preceding a proline residue.[55]

By employing three-dimensional TOCSY and NOESY experiments for the [^{15}N]IRAK1-UD, and aided by homonuclear TOCSY and NOESY spectra of an IRAK1-derived peptide encompassing residues P_{162}−K_{180} [$\text{IRAK1}^{162-180}$ (underlined in Figure 1A)], we were able to determine peak assignments for several residues in and around the $_{168}\text{WPPPP}_{172}$ motif (Table S1 of the Supporting Information). Several residues within the A165−S173 region exhibited distinct chemical shifts for the two isomers of the W_{168}−P_{169} peptide bond, and distinct *cis* (25%) and *trans* (75%) peaks were also observed for the isomers of the S_{173}−P_{174} peptide bond (Figure S1 of the Supporting Information). Assignments of the prolyl isomers of the W_{168}−P_{169} peptide bond were made both by identification of characteristic through-space NOEs to proline protons from the preceding residue's α proton ($d_{\alpha\delta}$ for the *trans* isomer and $d_{\alpha\alpha}$ for the *cis* isomer) and by exchange cross peaks in the ^{15}N ZZ-exchange experiment in the presence of the isomerase CypA, as described below.

These results, which represent the first structural information about the proline-rich IRAK1 undefined domain, show that this domain is conformationally heterogeneous. While the narrow chemical shift dispersion in the ^{15}N−^{1}H HSQC spectrum indicates rapid exchange between allowed regions of backbone conformational space, the additional peaks arising from *cis*−*trans* isomerization demonstrate that multiple sites undergo slow two-state exchange, adding to the conformational richness of this domain.

Determination of the IRAK1-UD Recognition Sequence and Isomer Specificity of Interaction with the VASP EVH1 Domain. When the [^{15}N]IRAK1-UD was titrated with the VASP EVH1 domain, six backbone peaks and one tryptophan side chain peak moved substantially. These peaks correspond to the NH groups of A165−A175 (proline residues in the sequence do not yield ^{15}N−^{1}H HSQC peaks) (Figure 2A,B). This demonstrates that binding is specific for the $_{168}\text{WPPPP}_{172}$ motif in the IRAK1-UD and that the interaction is in fast exchange on the NMR time scale[48] (~4000 s^{-1} in this case). As described above, this region of the IRAK1-UD sequence exhibits distinct peaks corresponding to the *cis* and *trans* states of the W_{168}−P_{169} peptide bond. While the peaks corresponding to the *trans* isomer of the W_{168}−P_{169} peptide bond move substantially upon binding, the *cis* isomer peaks simply decrease in intensity as the EVH1 domain is added, indicating that the interaction is specific for the *trans* isomer (Figure 2A,B). Therefore, a coupled equilibrium model that includes both *cis*−*trans* isomerization and binding (Figure 2C) is indicated for this system. This result is consistent with the crystal structures of both the EVH1 domain of Mena[49] and

dx.doi.org/10.1021/bi500031e | *Biochemistry* 2014, 53, 3593−3607

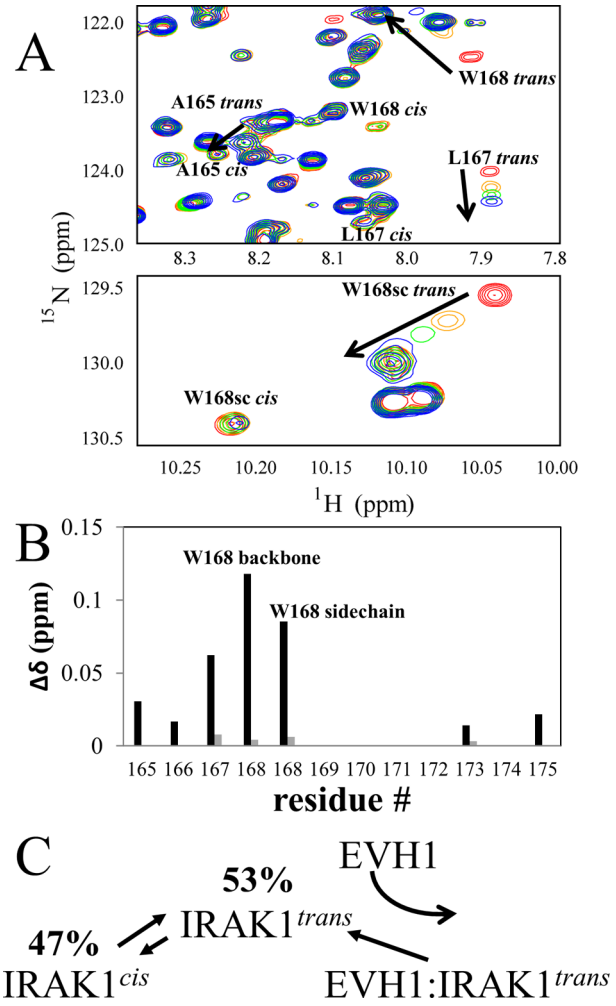

Figure 2. IRAK1-UD/VASP-EVH1 interaction is *trans*-specific. (A) When the ^{15}N-labeled IRAK1-UD is titrated with the unlabeled VASP EVH1 domain in a series of ^{15}N−^{1}H HSQC spectra, *trans* isomer peaks shift between free and bound positions, while peaks corresponding to the *cis* isomer only decreases in intensity. Colors represent the progression of the EVH1 domain concentration, with red representing data for apo IRAK1-UD and blue for the highest EVH1 domain concentration. The top panel shows a portion of the backbone amide region of the ^{15}N−^{1}H HSQC series, and the bottom panel shows the tryptophan side chain region of the spectra. (B) Composite chemical shift changes of backbone and side chain amides of IRAK1 residues 165−175 between the apo and final spectra of the EVH1 domain/[^{15}N]IRAK1-UD titration. Black bars represent peaks corresponding to the *trans* isomer of W168−P169, and gray bars represent peaks for the *cis* isomer, for peaks that were discernible in the final spectrum. (C) Three-state population shift model, including *cis*−*trans* isomerization in the IRAK1 protein and *trans*-specific binding, used to interpret and fit IRAK1/EVH1 domain binding data.

Evl[56] bound to ActA peptides, which show a *trans* peptide bond between the phenylalanine and the first proline of the bound FPPPP sequence.

Determination of the Thermodynamics and Kinetics of the Interaction between the IRAK1-UD and the VASP EVH1 Domain. To measure the affinity and kinetics of binding between the IRAK1-UD and the VASP EVH1 domain, the [^{15}N]EVH1 domain was titrated with the unlabeled IRAK1$^{162-180}$ peptide (Figure 1A). Use of IRAK1$^{162-180}$ rather than the full IRAK1-UD was preferred because of its solubility (allowing saturation of the [^{15}N]EVH1 domain to be approached) and its negligible contribution to the molecular weight of the bound complex. This titration yielded several resolved peak trajectories (Figure 3A), indicating fast exchange

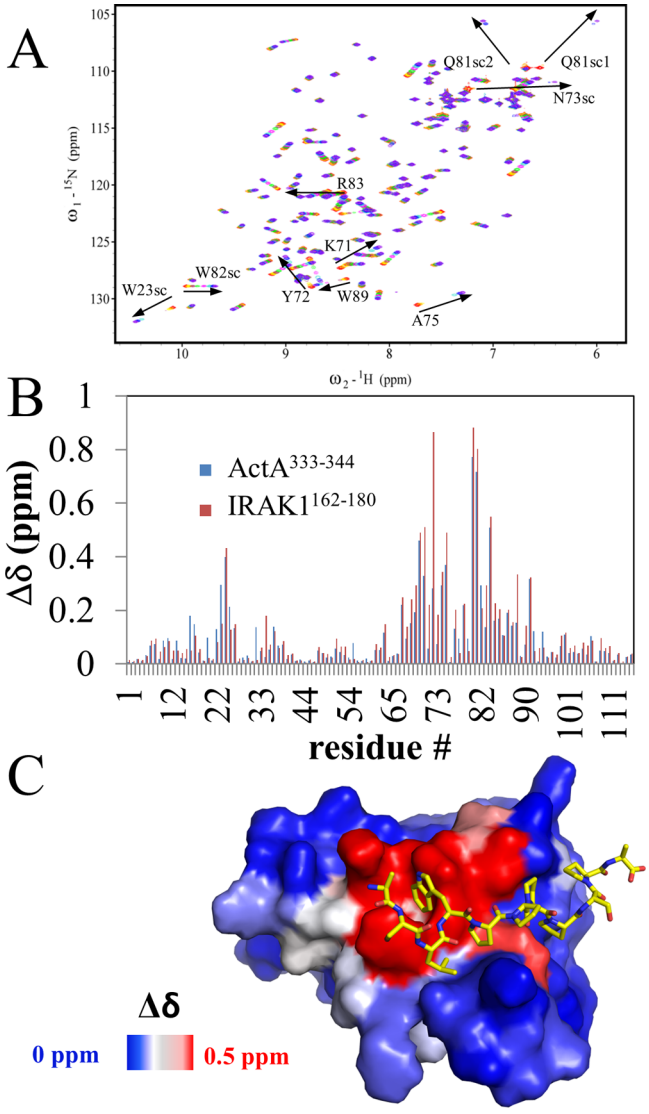

Figure 3. Chemical shift mapping to EVH1 structure. The [^{15}N]EVH1 domain was titrated with the IRAK1-derived peptide IRAK1$^{162-180}$, and a series of ^{15}N−^{1}H HSQC spectra (A) were recorded. Colors indicate peptide concentrations, undergoing a transition between free (red) and bound (purple) EVH1 domain. (B) Composite chemical shift changes for [^{15}N]EVH1 peaks between apo and peptide-bound positions. Chemical shift changes for IRAK1$^{162-180}$ titration are colored red and changes for ActA$^{333-344}$ titration blue. (C) Representation of the solution structure of the VASP EVH1 domain (PDB entry 1EGX[28]) with the IRAK1 peptide-induced chemical shift perturbations mapped to it. For each residue, the surface representation is colored according to the greater of the chemical shift changes of the backbone and side chain amide. Images were generated using the surface view representation and colored according to chemical shift perturbation using the data2bfactor.py and color_b.py scripts from R. L. Campbell's PyMol script repository at Queen's University [Kingston, ON (http://pldserver1.biochem.queensu.ca/~rlc/work/pymol/)] in PyMOL.[93] The peptide was modeled into the binding site by homology with the crystal structure of the Mena EVH1 domain bound to an ActA-derived peptide (PDB entry 1EVH[49]).

dx.doi.org/10.1021/bi500031e | *Biochemistry* 2014, 53, 3593−3607

on the NMR time scale as was observed from the ^{15}N-labeled IRAK1-UD perspective (Figure 2). Using the peak assignments for the VASP EVH1 domain (BioMagResBank accession number 18569[28]), we observed that the pattern of chemical shift perturbations across the EVH1 domain sequence upon addition of IRAK1$^{162-180}$ closely matches that observed for the FPPPP motifs of ActA binding to the VASP EVH1 domain.[28] This was confirmed by titrating the [^{15}N]EVH1 domain with an ActA-derived peptide ActA$^{333-344}$ ($_{333}$FEFPPPPTEDEL$_{344}$) and comparing chemical shift perturbations (Figure 3B). This suggests that IRAK1$^{162-180}$ binds in the same orientation displayed by published structures of Ena/VASP EVH1 domain peptide complexes.[49,56] The largest perturbations arose from residues (e.g., W23 side chain, K71, Y72, N73 side chain, A75, Q81 side chain, and R83) in the binding surface defined by the crystal structure of the Mena EVH1 domain/ActA complex,[49] as illustrated by mapping chemical shift perturbations to the EVH1 domain solution structure[28] (Figure 3C). Analysis of 21 ^{1}H and 21 ^{15}N chemical shift data sets yielded an apparent dissociation constant (K_D^{App}) of 203 ± 3 μM (example fits are shown in Figure 4A). This apparent affinity corresponds to a

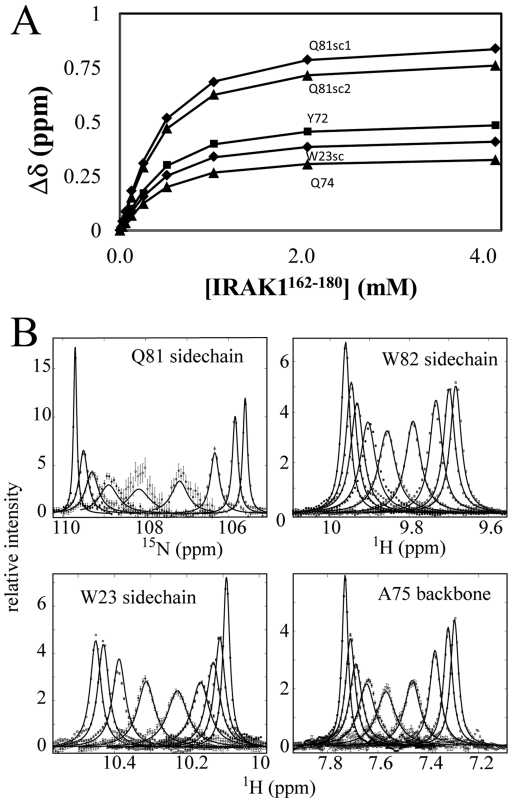

Figure 4. Measurement of the affinity and kinetics of binding between the VASP EVH1 domain and an IRAK1-derived peptide. (A) Composite chemical shift changes between free and bound states for selected EVH1 peaks as a function of peptide concentration (symbols). The data were fit (solid lines) to obtain an apparent dissociation constant (K_D^{App}) of the interaction of 203 ± 3 μM. (B) NMR line shape analysis of selected EVH1 peaks in the peptide titration series. 1D slices through the centers of [^{15}N]EVH1 domain peaks were extracted along the ^{15}N or ^{1}H dimension, and the data (symbols) were fit (solid lines) to yield on and off rates for the *trans*-specific interaction: k_{on} = (3.7 ± 0.1) × 10^7 M^{-1} s^{-1}, and k_{off} = 4000 ± 200 s^{-1}, where $k_{on} = k_{off}/K_D^{trans}$.

K_D^{trans} of 109 ± 4 μM, adjusted for coupling to the *cis*−*trans* equilibrium (Figure 2D) by

$$K_D^{App} = K_D^{trans}(1 + 1/K_{isom}) \quad (5)$$

where K_D^{trans} is the dissociation constant of the *trans* isomer of IRAK1 binding to the EVH1 domain and K_{isom} is the ratio of *trans* to *cis* for the free W$_{168}$−P$_{169}$ peptide bond as determined above. Titration of the [^{15}N]EVH1 domain with the full-length IRAK1-UD yielded a K_D^{App} of 280 ± 20 μM (data not shown). This reasonable agreement further validated the use of the peptide.

Line shape analysis of the titration data given above was employed to determine the on and off rates of the *trans* isomer of the IRAK1-UD binding to the VASP EVH1 domain, as described previously[45] and in Materials and Methods. The [^{15}N]EVH1 domain peaks that move the most in response to IRAK1$^{162-180}$ binding all display a similar pattern of broadening at intermediate titration points before narrowing as saturation is reached (Figure 4B). This exchange broadening is dependent on the difference in chemical shift and the time scale of exchange between the free and bound states. Each peak that is resolved throughout the titration therefore potentially provides two independent measures of the binding kinetics via the peak line shapes, one in the ^{1}H dimension and one in the ^{15}N dimension. Analysis of four line shape data sets (A75-^{1}H, W23sc-^{1}H, W82sc-^{1}H, and Q81sc-^{15}N) yielded a k_{off} of 4000 ± 200 s^{-1} and a k_{on} of (3.7 ± 0.1) × 10^7 M^{-1} s^{-1} (Figure 4B). This on rate is near the diffusion limit, as is common for interactions with proline-rich sequences.[57] Repeating this analysis with the [^{15}N]EVH1/ActA$^{333-344}$ data (data not shown) yielded a substantially higher affinity (14 μm) and on rate [k_{on} = (1.2 ± 0.1) × 10^8 M^{-1} s^{-1}, however, suggesting that electrostatic steering by the negative charges in this ActA sequence can contribute to the binding rate and affinity.

Demonstration of Cyclophilin A Catalysis of W$_{168}$−P$_{169}$ Peptide Bond Isomerization by NMR Spectroscopy. To test whether CypA catalyzes isomerization of the W$_{168}$−P$_{169}$ peptide bond in IRAK1, we applied two-dimensional ^{15}N ZZ-exchange NMR experiments to 0.8 mM [^{15}N]IRAK1-UD in the presence of 8 μM CypA (Figure 5A). ^{15}N ZZ-exchange spectroscopy allows for the identification and measurement of conformational exchange in the range between ∼0.1 and 10 s^{-1}.[51] Because the lower limit of this rate regime is approximately 1−2 orders of magnitude faster than typical uncatalyzed *cis*−*trans* isomerization rates,[55] intrinsic (uncatalyzed) *cis*−*trans* isomerization exchange is not detected in this experiment, but catalyzed isomerization can be detected. If two peaks display mutual cross peaks in an ^{15}N ZZ-exchange spectrum, it indicates that the same nucleus exchanges between two distinct states, and monitoring the cross peak intensity as a function of mixing time allows for measurement of the exchange rate.[51] In the ^{15}N ZZ-exchange spectra of the [^{15}N]IRAK1-UD, exchange cross peaks between many pairs of *cis* and *trans* isomers of X-Pro motifs throughout the sequence were observed in the presence of but not in the absence of CypA, indicating both the general lack of sequence specificity of CypA activity[58,59] and the high conformational heterogeneity of the proline-rich IRAK1-UD (Figure 5A). CypA-catalyzed isomerization of the $_{168}$WPPPP$_{172}$ motif was quantified using the resolved W$_{168}$ indole NH *cis* and *trans* peaks that show unambiguous exchange cross peaks (Figure 5A). Analysis of these W$_{168}$ indole NH exchange cross peaks and autopeaks yielded the catalyzed *cis*-to-*trans* (k_{CT} = 0.83 ±

dx.doi.org/10.1021/bi500031e | *Biochemistry* 2014, 53, 3593−3607

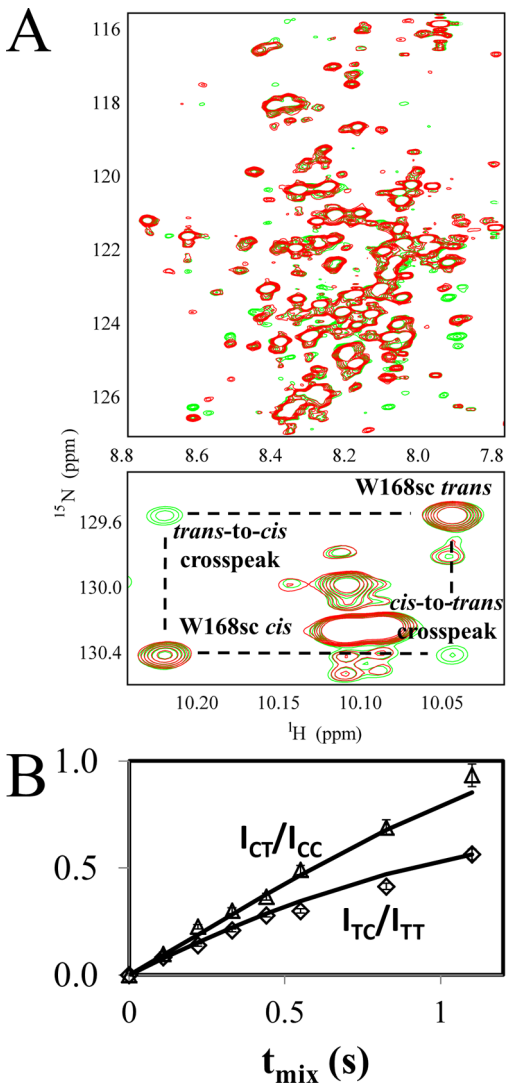

Figure 5. Cyclophilin A catalyzes the isomerization between *cis* and *trans* isomers of W168−P169 in IRAK1. (A) ^{15}N ZZ-exchange spectra of the [^{15}N]IRAK1-UD with a catalytic (8 μM) concentration of CypA. The red spectrum is taken with a mixing time of 0, while the green spectrum is a summation of multiple spectra with mixing times of 0.11, 0.22, 0.33, 0.44, 0.55, 0.83, and 1.10 s. The green spectrum shows cross peaks between pairs of peaks of *cis*−*trans* isomers in the sequence. The top panel shows a section of the backbone amide region and the bottom panel the tryptophan indole region, featuring the W168 side chain peaks. (B) Plot of normalized W168sc cross peak intensities (cross peak divided by autopeak) from the ^{15}N ZZ-exchange experiment as a function of mixing time. Data points are shown as symbols and fits as lines.

0.05 s^{-1}) and *trans*-to-*cis* (k_{TC} = 0.72 ± 0.04 s^{-1}) isomerization rates (Figure 5B). The enzyme concentration in this experiment (8 μM CypA) was chosen so that isomerization would be in this range, as cross peaks are too small to resolve at lower isomerization rates and the peaks would begin to broaden at higher rates, complicating analysis. This regime provides the added advantage that rates can be estimated from the initial slopes of the cross peak intensities divided by autopeak intensities.[60]

Tryptophan Fluorescence Allows Measurement of Uncatalyzed Prolyl Isomerization and Activation Enthalpy of the W_{168}−P_{169} Peptide Bond. In contrast to ^{15}N ZZ-exchange spectroscopy, fluorescence spectroscopy can be used to measure slow (τ > 10 s) processes like uncatalyzed prolyl isomerization.[45,54,61] Tryptophan fluorescence was employed to measure the kinetics of equilibration over the isomerization time scale, because both the VASP EVH1 domain and IRAK1$^{162-180}$ contain tryptophan residues in or near the interaction interface. The exquisite sensitivity of tryptophan fluorescence to local environment provides the potential for measuring differences not just between free and bound states but also between the *cis* and *trans* isomers of the W_{168}−P_{169} peptide bond in free IRAK1$^{162-180}$. Observation of the *cis*−*trans* isomerization kinetics is possible if the *cis* and *trans* populations can be significantly perturbed from their equilibrium values, and their return to equilibrium can be monitored. The strict specificity of the VASP EVH1 domain/IRAK1-UD interaction for the *trans* isomer of the W_{168}−P_{169} peptide bond provides a mechanism for perturbing this equilibrium, allowing either enrichment of the free *cis* isomer by rapid mixing of the two binding partners at a high concentration ([IRAK1$^{162-180}$] and [VASP EVH1] ≥ K_D^{App}) or enrichment of the free *trans* isomer by rapid dilution of the complex to a low concentration ([IRAK1$^{162-180}$] and [VASP EVH1] < K_D^{App}). In either case, the temporal separation of the fast binding reaction and slow prolyl isomerization allows detection and quantification of the slow, rate-limiting isomerization process.

When the IRAK1$^{162-180}$ peptide is mixed with excess VASP EVH1 domain, the 53% population of the *trans* conformation rapidly reaches its binding equilibrium with the EVH1 domain, and the free *trans* conformation is depleted relative to the free *cis* conformation. Subsequent conversion of the *cis* conformation to the *trans* conformation (toward equilibrium) provides additional *trans* conformation that binds, generating a time-dependent fluorescence signal that can reflect both equilibration of isomer populations of the free peptide and the additional isomerization-dependent binding. The initial binding phase (to the initial 53% *trans* conformation) cannot be observed because it is too fast (4000 s^{-1} as determined by NMR above) to be resolved under the experimental conditions, even in stopped-flow experiments. To implement this mixing experiment, 2 μL of 53 mM IRAK1$^{162-180}$ peptide was added to 2 mL buffer (final concentration of 53 μM IRAK1$^{162-180}$) containing a high concentration of the EVH1 domain (100 μM) in a quartz cuvette, and a fluorescence signal time course was recorded. The observed slow increase in tryptophan fluorescence was well fit by a single exponential with a rate constant of 0.0025 s^{-1} (Figure 6A). Notably, the observed change in the fluorescence signal could reflect time-dependent binding (rate-limited by prolyl isomerizion), the isomerization of the free peptide itself, or a combination of both.

Direct observation of changes in the fluorescence signal due to isomerization of the free peptide was achieved using a dilution approach. When the preformed VASP EVH1 domain/IRAK1$^{162-180}$ complex is diluted to a concentration below the K_D^{App}, the complex will rapidly dissociate, releasing the peptide. The released peptide is far from the *cis*−*trans* equilibrium, with high *trans* and low *cis* populations. The return of these populations to their equilibrium values can be monitored by tryptophan fluorescence if the *cis* and *trans* isomers produce different fluorescence signals. This approach unambiguously detects the prolyl isomerization kinetics independent of the binding reaction kinetics, because isomerization is temporally well separated from the rapid initial dissociation of the diluted

dx.doi.org/10.1021/bi500031e | *Biochemistry* 2014, 53, 3593−3607

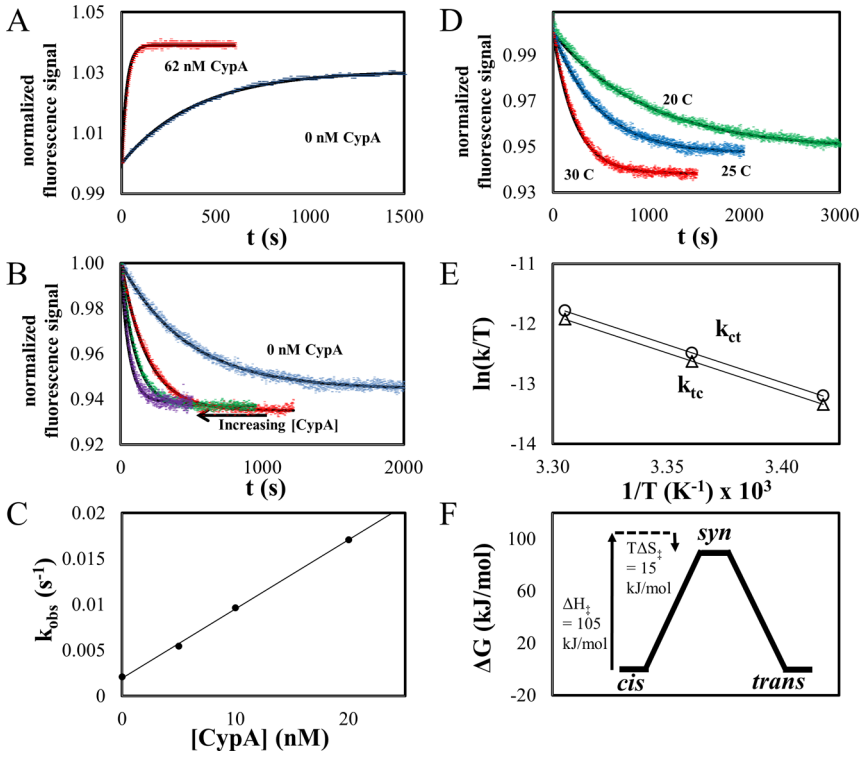

Figure 6. Tryptophan fluorescence shows cyclophilin A accelerates IRAK1-UD/EVH1 domain binding and equilibration of IRAK1 isomers. (A) Mixing the IRAK1$^{162-180}$ peptide with an excess of the VASP EVH1 domain yields a slow increase in the magnitude of the tryptophan fluorescence signal that reflects both binding and isomerization. Including CypA in the mixture accelerates this equilibration. (B) Diluting a concentrated stock of IRAK1$^{162-180}$ mixed with the VASP EVH1 domain to below the K_D^{App} of the interaction results in a slow decrease in the magnitude of the fluorescence signal that reflects isomerization of the unbound peptide. CypA accelerates the equilibration of isomers. (C) Dependence of the rate constant of equilibration in the dilution experiment, k_{obs}, on CypA concentration. (D) Performing the dilution experiment at different temperatures shows a strong dependence of k_{obs} on temperature. (E) Erying plots of the *cis*-to-*trans* and *trans*-to-*cis* rates (k_{CT} and k_{TC}, respectively) used to obtain the activation enthalpy and entropy of IRAK1$^{162-180}$ isomerization. (F) Energy diagram describing *cis* and *trans* isomers of W168−P169 in the IRAK1-UD. The activation enthalpy and entropy for the *cis*-to-*trans* transition are specified for 37 °C.

complex, and subsequent binding is negligible at such dilute concentrations.

To implement this approach, a concentrated mixture of 1 mM VASP EVH1 domain and 1 mM IRAK1$^{162-180}$ was allowed to fully equilibrate (≥1 h), and then 4 μL of this mixture was diluted into the cuvette for a final concentration of 2 μM EVH1 and peptide, well below the K_D^{App}. Fast dissociation of the bound *trans* peptide occurred in the dead time of the instrument, while slow equilibration of the *cis* and *trans* isomers of the free peptide was observed as a gradual decrease in the magnitude of the tryptophan fluorescence signal over the course of 1 h at 25 °C. This demonstrates that the *trans* isomer of the free peptide indeed produces a fluorescence intensity higher than that of the *cis* isomer, allowing direct detection of the isomerization kinetics. The data were well fit by a single exponential, yielding a k_{obs} of 0.00211 s^{-1} (in good agreement with the mixing experiment). The corresponding intrinsic *cis*-to-*trans* (k_{CT}) and *trans*-to-*cis* (k_{TC}) rates of isomerization are 0.00113 and 0.00098 s^{-1}, respectively, calculated as described in Materials and Methods. Inclusion of 5, 10, and 20 nM cyclophilin A in the dilution experiment accelerated isomerization by 2-, 4-, and 8-fold, respectively, displaying a linear dependence on CypA concentration as expected (Figure 6B,C). In addition to the ability to directly observe the isomerization process, this experiment has the important advantages of using ∼50-fold less material than the mixing experiment, and avoiding the inner-filter effect (to which the mixing experiment is susceptible).

To measure the activation enthalpy of $W_{168}-P_{169}$ peptide bond isomerization, the dilution fluorescence experiment was performed at different temperatures (Figure 6D,E). The extraction of individual k_{CT} and k_{TC} isomerization rates from the measured k_{ex} was accomplished using a constant value of 1.15 for K_{isom}, justified by homonuclear 1D and TOCSY spectra of IRAK1$^{162-180}$ that show no temperature dependence of this parameter. These rates were fit to the linear form of the Eyring−Polanyi equation:[62]

$$\ln(k_{CT,TC}/T) = -\Delta H_{‡}^{CT,TC}/(RT) + \ln(k_B/h) + \Delta S_{‡}^{CT,TC}/R \quad (6)$$

where T is the temperature, R is the gas constant, k_B is the Boltzmann constant, h is Planck's constant, and $\Delta H_{‡}^{CT,TC}$ and $\Delta S_{‡}^{CT,TC}$ are the activation enthalpy and entropy, respectively, of *cis*-to-*trans* (CT) and *trans*-to-*cis* (TC) isomerization. Fitting to this equation yields slopes that correspond to activation enthalpies of 105 kJ/mol for both the *trans*-to-*cis* and *cis*-to-*trans* conversions and intercepts that correspond to activation entropies of 48 and 49 J K^{-1} mol^{-1} for the *trans*-to-*cis* and *cis*-to-*trans* conversions, respectively (Figure 6E,F). Extrapolation to physiological temperature (37 °C) yields the population of *trans* (53%) and the uncatalyzed isomerization rate (k_{ex} = 0.011 s^{-1}). The activation enthalpies and entropies of the *cis*-to-*trans* transition at 37 °C are illustrated in an energy diagram (Figure 6F).

dx.doi.org/10.1021/bi500031e | *Biochemistry* 2014, 53, 3593−3607

Tryptophan Fluorescence Shows That Cyclophilin A "Catalyzes" VASP EVH1 Domain Interactions. Inclusion of CypA in the mixing experiment described earlier can be expected to accelerate completion of the *trans*-specific VASP EVH1 domain/IRAK1$^{162-180}$ binding reaction, after the initial binding of the preexisting *trans* isomer. In fact, inclusion of 62 nM cyclophilin A in this mixing experiment accelerated the reaction approximately 15-fold (Figure 6A). However, because changes in the *cis* and *trans* populations give rise to changes in the fluorescence signal, it is difficult to distinguish between the fluorescence signal due solely to isomerization of the free peptide (which would dominate if binding did not give rise to substantial differences in the fluorescence signal, or if the VASP EVH1 domain is not in excess) and the fluorescence signal representing CypA-accelerated binding to the VASP EVH1 domain. Thus, while in principle the mixing experiment should provide the opportunity to observe "CypA-catalyzed binding" of this *trans*-specific interaction, the contribution of isomerization of the free peptide to the observed fluorescence signal precludes detection of a signal dependent solely on binding.

To directly observe CypA acceleration of binding of the VASP EVH1 domain to a binding partner, the mixing experiment described above was performed using the ActA$^{333-344}$ peptide, which also partitions into *cis* (25%) and *trans* (75%) isomers (Figure S2 of the Supporting Information). This sequence contains a phenylalanine instead of tryptophan in the binding motif, and therefore, tryptophan fluorescence experiments are not sensitive to prolyl isomerization of the free peptide. By contrast, Trp23 in the EVH1 domain binding surface is shielded in the complex relative to the apo domain, so fluorescence experiments with this peptide are still sensitive to binding. Titrating the EVH1 domain with this peptide shows that the magnitude of the tryptophan fluorescence signal of EVH1 increases >34% upon binding (Figure 7A). Mixing ActA$^{333-344}$ with an excess of the EVH1 domain produced an immediate large increase in tryptophan fluorescence followed by a smaller, slow increase, following an exponential expression with a rate of 0.0038 s^{-1} (Figure 7B). This slow phase can be unambiguously interpreted as prolyl isomerization-limited binding, because the only tryptophan fluorescence signal arises from the EVH1 domain in this case. This measured rate corresponds to the intrinsic *trans*-to-*cis* (0.0012 s^{-1}) and *cis*-to-*trans* (0.0035 s^{-1}) isomerization rates (Table 1) according to eq 4. Equation 4 accounts for coupling between isomerization and binding by scaling the intrinsic *trans*-to-*cis* rate by the fraction of free peptide. Inclusion of 62 nM CypA in the mixture accelerated the reaction as expected, by 10-fold (Figure 7B). This provides a direct example of a prolyl isomerase, CypA, accelerating an interaction between the VASP EVH1 domain and one of its binding partners.

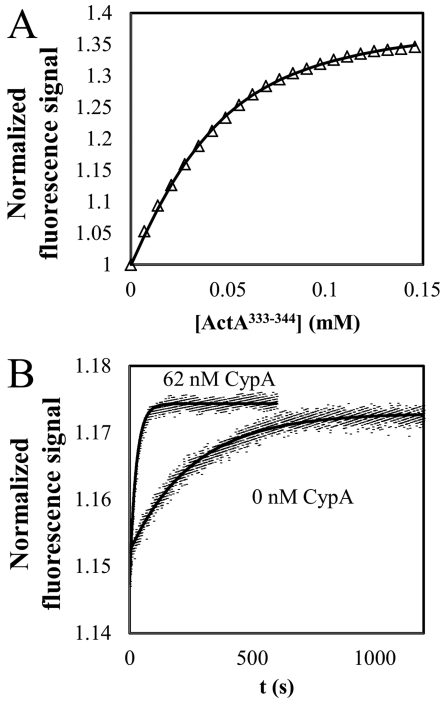

Figure 7. Tryptophan fluorescence shows CypA accelerates ActA/EVH1 domain binding. (A) The tryptophan fluorescence signal of the VASP EVH1 domain increases upon binding of ActA$^{333-344}$, allowing independent measurement of the binding constant (K_D^{trans} = 17 μM, compared to 14 μM by NMR). Data are shown as symbols, and a fit is shown as a solid line. (B) Mixing an excess of the EVH1 domain with ActA$^{333-344}$ results in a slow binding phase that can be accelerated with a catalytic quantity (62 nM) of CypA.

Table 1. Rates and Equilibrium and Binding Constants for IRAK1$^{162-180}$ and ActA$^{333-340}$

	IRAK1$^{162-180}$	ActA$^{333-344}$
k_{CT} (s^{-1})	0.00113	0.0035
k_{TC} (s^{-1})	0.00098	0.0012
[*trans*]/[*cis*]	1.15 ± 0.08	3.0
k_{off} (s^{-1})	4000 ± 200	1800 ± 200
k_{on} (M^{-1} s^{-1})	(3.7 ± 0.1) × 10^7	(1.2 ± 0.1) × 10^8
K_D^{trans} (μM)	109 ± 4	14 ± 1

DISCUSSION

Here, we have applied biophysical methods to investigate and quantify binding between the EVH1 domain of VASP and the undefined domain of IRAK1. Using purified components, we have demonstrated that the VASP EVH1 domain binds to the $_{168}$WPPPP$_{172}$ motif in the IRAK1-UD, with specificity for the *trans* isomer of the W_{168}–P_{169} peptide bond. Our studies provide a quantitative thermodynamic and kinetic description of the coupled equilibrium between W_{168}–P_{169} *cis*–*trans* isomerization and IRAK1-UD/VASP EVH1 domain binding (Table 1) and demonstrate how acceleration of isomerization by CypA effectively catalyzes binding. These results provide important insights into a potential role of *cis*–*trans* isomerization in innate immunity signaling and offer a possible direct physical mechanism for connecting IRAK1-mediated signaling pathways to VASP-mediated regulation of actin cytoskeletal dynamics. The extension of our studies to the interaction between the VASP EVH1 domain and the *L. monocytogenes* surface protein ActA (Table 1) suggests that isomerase-catalyzed binding in isomer-selective interactions is generally applicable to other systems. In this broader context, catalysis of the rate-limiting isomerization step in an isomer-specific binding reaction represents a largely overlooked function for peptidyl prolyl isomerase enzymes.

The *trans*-specific IRAK1-UD/VASP EVH1 domain interaction characterized here can be rationalized by considering the details of the canonical EVH1 domain/ligand interaction interface. EVH1 domains employ a conserved network of aromatic and polar side chains to directly interact with the carbonyl groups of their proline-rich binding motifs.[63] In VASP, two side chains, Gln81 and Trp23, are positioned to hydrogen

dx.doi.org/10.1021/bi500031e | *Biochemistry* 2014, 53, 3593–3607

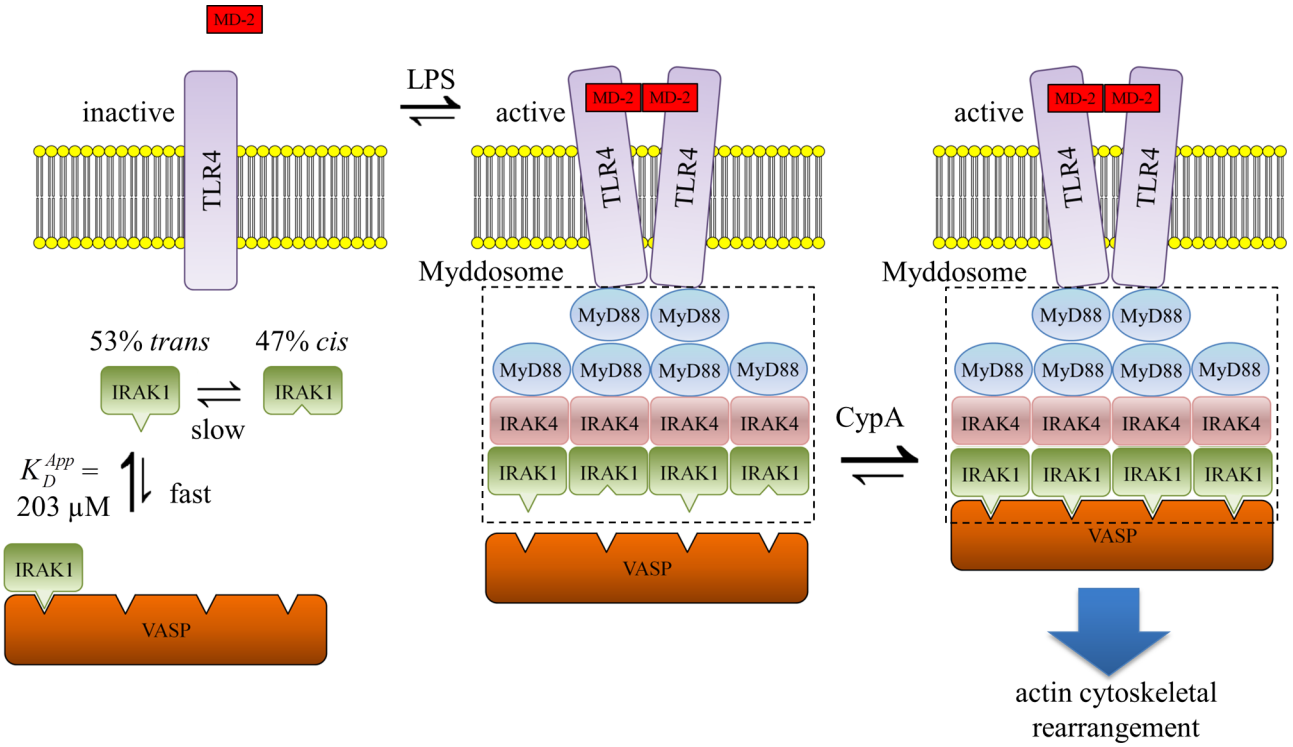

Figure 8. Model for hypothesized direct coupling of Toll/IL-1 receptor signaling to actin cytoskeletal rearrangement. In the left panel, when receptors are inactive, the interaction between IRAK1 and VASP is weak (K_D^{App} = 203 μM). Because cellular concentrations of IRAK1 and VASP are lower than this K_D^{App} value, the influence of their interaction should be negligible. In the middle panel, activation of the Toll/IL-1 receptor [e.g., lipopolysaccharide (LPS) activation of TLR4 via MD-2, as shown] induces tetramerization of IRAK1 via formation of the Myddosome (in the box, six MyD88, four IRAK4, and four IRAK1 subunits). An average of two of the four IRAK1 subunits in a given tetramer will be in the *trans* conformation of the W_{168}–P_{169} peptide bond and capable of interaction with the tetrameric *trans*-selective VASP EVH1 domain, yielding a rapid but partial avidity enhancement, with full avidity achieved on the slower time scale of *cis*–*trans* isomerization. In the right panel, catalysis by an isomerase enzyme such as CypA achieves rapid full avidity enhancement of the interaction, effectively linking Toll/IL-1 receptor signaling to actin cytoskeletal rearrangement via interaction between IRAK1 and VASP.

bond with the carbonyl oxygens of the first proline and third residue (x) in the (W/F)PxφP motif, respectively. Furthermore, a hydrophobic pocket defined by the side chain methylenes K71, N73, Q81, and R83 accommodates a hydrophobic aromatic like tryptophan or phenylalanine or, to a smaller degree, the aliphatic leucine.[28,49,56] Flipping the W/F–P peptide bond to the *cis* isomer while constraining the two hydrogen bonds causes the side chain of the first residue to flip away from the binding surface (Figure S3 of the Supporting Information). Thus, the fact that optimal binding requires both that the side chain of the first residue insert into this pocket and the carbonyls of the second and third residues hydrogen bond to side chains in the EVH1 domain can explain the result that binding is specific for the *trans* isomer of the W/F–P peptide bond.

The affinity of the IRAK1/VASP monomer/monomer interaction quantified here is relatively weak (K_D^{App} = 203 ± 3 μM). However, a logical mechanism by which this interaction could be regulated is the oligomerization of IRAK1, because VASP functions as a constitutive tetramer.[64] Avidity can increase the affinity of a relatively weak 1:1 interaction to an exponentially enhanced multimer/multimer interaction.[65] The activation of both TLR and IL-1R family members induces their dimerization.[66,67] In mammals, the subsequent intracellular signaling steps include the assembly of a multiprotein complex called the Myddosome (Figure 8), nucleated by the intracellular TIR domains of the receptors. A recent crystal structure suggests that six MyD88 molecules bind the clustered receptor TIR domains and initiate a helical array onto which the death domains of four IRAK4 molecules and then four IRAK1 (or IRAK2) molecules assemble.[16] This receptor-initiated tetramerization of IRAK1 may significantly increase the extent of the interaction with the constitutively tetrameric VASP (Figure 8). Receptor oligomerization has long been understood to be an important mechanism in signal transduction,[68,69] especially in the context of the immune system.[70,71] In some cases, ligand-induced oligomerization of a receptor is important for transducing a signal in a kind of "oligomerization cascade", in which formation of a receptor-initiated multimeric complex induces the subsequent oligomerization of downstream binding partners.[72,73]

In the context of a putative tetrameric form of IRAK1, the conformation-selective IRAK1/VASP interaction also has important implications for the kinetics of binding. Because the theoretically tightest interaction is between two tetramers, the fact that the WPPPP binding site partitions into 47% *cis* and 53% *trans* isomers means the tightest interaction would only initially arise for $(0.53)^4$ = 8% of the total available IRAK1 tetramers. Minutes would be required for additional subunits to convert to the *trans* isomer in the absence of PPIase activity. A cytoplasmic prolyl isomerase such as CypA may therefore play a role in the proper function of VASP interactions by "catalyzing binding" to its partners, allowing full avidity enhancement to be achieved on the millisecond time scale (Figure 8). This principle can be generalized to other isomer-specific interactions between oligomers. For example, even the

dx.doi.org/10.1021/bi500031e | *Biochemistry* 2014, 53, 3593–3607

more modest 25% *cis* conformation as determined here for one of the four tandem FPPPP motifs in ActA corresponds to only $(0.75)^4$ = 32% ActA molecules with all four motifs simultaneously in the *trans* state. An analogy can be drawn to protein folding, in which the isomerization of multiple proline residues in the fold of a protein can collectively contribute to folding kinetics.[74]

The involvement of CypA in facilitating a rapid response in specific signaling pathways has previously been demonstrated. In addition to its role as a foldase,[75] there are growing examples of specific functions for CypA in cell signaling, particularly in immune cells. CypA regulates a conformational switch in interleukin-2 tyrosine kinase (Itk) by isomerizing a proline in the Itk SH2 domain, allowing interconversion between active and inactive states.[76] In another example, CypA isomerizes a conformational switch in the adaptor protein Crk, also accelerating conversion between inactive and active conformations.[77] The isomerase activity of CypA has also been found to be required for cytokinesis in Jurkat cells.[78] Our results showing that the W_{168}–P_{169} peptide bond in the IRAK1-UD partitions into populations of 47% *cis* and 53% *trans*, that only the *trans* isomer participates in binding to the VASP EVH1 domain, and that CypA accelerates the completion of this 1:1 interaction suggest another possible use of PPIase-catalyzed isomerization as a molecular switch in innate immunity signaling.

The WPPPP motif in IRAK1 is the only established biological VASP binding site that features a tryptophan instead of a phenylalanine. However, multiple peptide binding studies have demonstrated a preference of the VASP EVH1 domain for WPxφP over FPxφP motifs.[26,28] It should be noted that phenylalanine is only lower than tryptophan and tyrosine in its tendency to stabilize the *cis* isomer when preceding a proline residue.[55] Therefore, the nearly equal populations of the *cis* and *trans* isomer states the potential for isomer-specific binding events are important considerations for FPxφP motifs as well as the WPxφP motif described here. Notably, a conformation-selective interaction with one state in a nearly degenerate two-state conformational equilibrium (i.e., a three-state population shift model such as that characterized here) has been shown to impart optimal properties for signal transmission.[79,80] Briefly, a degenerate conformational equilibrium allows rapid conformation-specific binding while still displaying a meaningful change (a shift in conformational populations) in response to binding. The near degeneracy of prolyl *cis* and *trans* states, such as in sequence motifs that contain WP, FP, or YP in flexible regions of proteins, could optimize the regulation of distinct functions associated with the *cis* and *trans* isomers, for example, active and inactive states. Indeed, CypA-catalyzed isomerization between prolyl isomer-coupled conformational states (60% *trans* and 40% *cis*) in the SH2 domain of ITK allows rapid shifts between active and inactive ITK states in response to isomer-selective binding, although in this case the *cis* population is stabilized by protein structure rather than the amino acid preceding proline.[81]

It is informative to note that binding between the FPPPP sequence motif and the EVH1 domain of Ena/VASP proteins has been previously shown to link receptor-activated signaling to rearrangement of the actin cytoskeleton. In one example, polarization of the actin cytoskeleton of helper T cells toward antigen-presenting cells upon T cell receptor (TCR) stimulation is dependent on the recruitment of Ena/VASP proteins to the TCR signaling complex via a FPPPP motif in the Fyb/SLAP protein.[82] In a similar example, phagocytosis in macrophages in response to Fc receptor stimulation[83] was shown to require Fyb/SLAP recruitment of Ena/VASP proteins to activated signaling complexes, logically mediated by binding of the EVH1 domain to a FPPPP motif in Fyb/SLAP.[84] This recruitment was shown to be necessary for the formation of the actin-based phagocytic cup and for the phagocytosis of opsonized red blood cells.[84] In both cases, the FPPPP-mediated interaction between Ena/VASP proteins and Fyb/SLAP is crucial to linking receptor activation to cytoskeletal remodeling. The VASP/IRAK1 interaction characterized *in vitro* here could provide a similar link between TLR- or IL-1R-mediated signaling and remodeling of the actin cytoskeleton via a prolyl *cis*–*trans* molecular switch.

The functional link between IRAK1-mediated TLR signaling pathways and the reorganization of the actin cytoskeleton is well-established. For example, stimulation of TLR4 with lipopolysaccharide induces cell migration[85] and phagocytosis[86] in macrophages. However, varied and complex mechanisms regulate this functional link, as exemplified by the fact that lipopolysaccharide can either enhance[87] or arrest[88] chemotaxis, depending on cell type and conditions. Our characterization here of the direct interaction between a component of the TLR signaling machinery (IRAK1) and a key regulator of the actin cytoskeleton (VASP) suggests that this physical link might be one element in this complex functional link.

It was recently reported that in human THP1 and MAT-2 cells, VASP and IRAK1 co-immunoprecipitate.[25] The same researchers also investigated IRAK1's involvement in phosphorylation of VASP by PKC. They found that in IRAK1-deficient murine bone marrow-derived macrophages, activation of PKC by PMA stimulation resulted in impaired migration and less sustained VASP phosphorylation than in wild-type cells.[25] These results seem to collectively suggest a key role for the VASP/IRAK1 interaction in macrophage migration. However, while human IRAK1 contains the WPPPP VASP binding motif we describe here, murine IRAK1 does not contain any such motif. In fact, the appearance of the WPPPP binding motif in human IRAK1 is due to an Arg-to-Trp point mutation that occurred very recently on an evolutionary time scale (Figure S4 of the Supporting Information). It is possible that this is a result of selective pressure, and indeed, genes in the immune system tend to evolve more rapidly because of their coevolution with pathogens.[89] Our demonstration of the direct interaction between the WPPPP motif in human IRAK1 and the VASP EVH1 domain suggests a possible recently evolved mechanism for linking innate immunity signaling to cytoskeletal rearrangement.

The quantification of intrinsic and PPIase-catalyzed peptidyl prolyl *cis*–*trans* isomerization rates for specific sequence motifs is central to gaining an in-depth understanding of this class of molecular switches. Here, we have employed tryptophan fluorescence to measure the intrinsic rate of isomerization of the W_{168}–P_{169} site in IRAK1. To the best of our knowledge, this is the first example of an experiment that takes advantage of the difference in tryptophan fluorescence intensities of the *cis* and *trans* isomers of the W–P dipeptide sequence to measure the kinetics of isomerization of an unstructured peptide. We have shown both that the isomerase CypA can accelerate isomerization of $IRAK1^{162-180}$ and also (using the tryptophan fluorescence of the EVH1 domain) that CypA isomerization of the related sequence in ActA can accelerate binding of ActA to the EVH1 domain. This represents a direct demonstration of an

underappreciated role of prolyl isomerases, the acceleration of isomer-specific protein/protein interactions.

CONCLUSIONS

The VASP/IRAK1 interaction provides an intriguing example of how, in a binding interaction with a proline motif, the binding kinetics can be substantially dependent on *cis*−*trans* isomerization. Binding between tetrameric VASP and a multivalent binding partner such as tetrameric IRAK1 assembled onto the Myddosome may be especially dependent on isomerization because the probability of a multivalent protein being all-*trans*, given by (% *trans*)^4, is lower than for a single binding site. Notably, this can be applied to other known VASP interaction partners such as zyxin,[90] lamellipodin,[91] and ActA,[92] which have four or five FPxφP motifs in tandem repeat, or vinculin, which oligomerizes.[34] Given the relatively weak affinity of the monomeric VASP EVH1 domain for its substrates (19−200 μM), as well as the tendency of VASP binding sites to exist as tandem repeats, it seems likely that avidity is a driving force for VASP interactions. Therefore, we suggest that a cytoplasmic isomerase such as CypA may be necessary for the proper function of VASP-mediated processes. However, future studies are needed to experimentally test this prediction.

ASSOCIATED CONTENT

Supporting Information

Chemical shift assignments of IRAK1 Residues A165-A175 for the *cis* and *trans* isomers of W168-P169 (Table S1), TOCSY data of IRAK1$^{162-180}$ used to assign residues A165−A175 of the IRAK1-UD (Figure S1), TOCSY data of ActA$^{333-344}$ used to measure the *cis* versus *trans* populations of the F335−P336 peptide bond (Figure S2), a structural model of IRAK1 bound to the EVH1 domain while adopting the *trans* or *cis* isomers (Figure S3), and an alignment of IRAK1 residues 130−208 in primates, showing that W168 is a recent mutation (Figure S4). This material is available free of charge via the Internet at http://pubs.acs.org.

AUTHOR INFORMATION

Corresponding Author

*E-mail: lkn2@cornell.edu. Phone: (607) 255-7208. Fax: (607) 255-6249.

Author Contributions

A.I.G. performed experiments and interpreted data. A.I.G. and L.K.N. wrote the manuscript. J.K. cloned the IRAK1-UD.

Funding

This work was supported by National Science Foundation Grant MCB-1157806 to L.K.N.

Notes

The authors declare no competing financial interests.

ACKNOWLEDGMENTS

We thank the Cornell University Protein Facility for providing us with expression vectors and for their help with preliminary stopped-flow experiments. We thank Kun Ping Lu for providing us with the original plasmid used to clone the IRAK1-UD. We thank the laboratories of Dyche Mullins and Michael Way for providing us with VASP expression materials. We thank Charalampos Kalodimos for providing us with CypA expression materials. We thank Soumya De for help purifying CypA. We thank Gerald Feigenson for the use of the fluorescence spectrophotometer.

ABBREVIATIONS

VASP, vasodilator-stimulated phosphoprotein; IRAK1, interleukin-1 receptor-associated kinase 1; EVH1, enabled/VASP homology 1; CypA, cyclophilin A; HSQC, heteronuclear single-quantum correlation spectroscopy; NMR, nuclear magnetic resonance; PPIase, peptidyl prolyl isomerase enzyme.

REFERENCES

(1) Moresco, E. M., LaVine, D., and Beutler, B. (2011) Toll-like receptors. *Curr. Biol. 21*, R488−R493.

(2) Carpenter, S., and O'Neill, L. A. (2009) Recent insights into the structure of Toll-like receptors and post-translational modifications of their associated signalling proteins. *Biochem. J. 422*, 1−10.

(3) McGettrick, A. F., and O'Neill, L. A. (2010) Regulators of TLR4 signaling by endotoxins. *Subcell. Biochem. 53*, 153−171.

(4) Uematsu, S., and Akira, S. (2007) Toll-like receptors and Type I interferons. *J. Biol. Chem. 282*, 15319−15323.

(5) Casanova, J. L., Abel, L., and Quintana-Murci, L. (2011) Human TLRs and IL-1Rs in host defense: Natural insights from evolutionary, epidemiological, and clinical genetics. *Annu. Rev. Immunol. 29*, 447−491.

(6) Martin, M. U., and Wesche, H. (2002) Summary and comparison of the signaling mechanisms of the Toll/interleukin-1 receptor family. *Biochim. Biophys. Acta 1592*, 265−280.

(7) Janssens, S., and Beyaert, R. (2003) Functional diversity and regulation of different interleukin-1 receptor-associated kinase (IRAK) family members. *Mol. Cell 11*, 293−302.

(8) Neumann, D., Kollewe, C., Resch, K., and Martin, M. U. (2007) The death domain of IRAK-1: An oligomerization domain mediating interactions with MyD88, Tollip, IRAK-1, and IRAK-4. *Biochem. Biophys. Res. Commun. 354*, 1089−1094.

(9) Park, H. H., Lo, Y. C., Lin, S. C., Wang, L., Yang, J. K., and Wu, H. (2007) The death domain superfamily in intracellular signaling of apoptosis and inflammation. *Annu. Rev. Immunol. 25*, 561−586.

(10) Flannery, S., and Bowie, A. G. (2010) The interleukin-1 receptor-associated kinases: Critical regulators of innate immune signalling. *Biochem. Pharmacol. 80*, 1981−1991.

(11) Song, K. W., Talamas, F. X., Suttmann, R. T., Olson, P. S., Barnett, J. W., Lee, S. W., Thompson, K. D., Jin, S., Hekmat-Nejad, M., Cai, T. Z., Manning, A. M., Hill, R. J., and Wong, B. R. (2009) The kinase activities of interleukin-1 receptor associated kinase (IRAK)-1 and 4 are redundant in the control of inflammatory cytokine expression in human cells. *Mol. Immunol. 46*, 1458−1466.

(12) Kawagoe, T., Sato, S., Jung, A., Yamamoto, M., Matsui, K., Kato, H., Uematsu, S., Takeuchi, O., and Akira, S. (2007) Essential role of IRAK-4 protein and its kinase activity in Toll-like receptor-mediated immune responses but not in TCR signaling. *J. Exp. Med. 204*, 1013−1024.

(13) Koziczak-Holbro, M., Joyce, C., Gluck, A., Kinzel, B., Muller, M., Tschopp, C., Mathison, J. C., Davis, C. N., and Gram, H. (2007) IRAK-4 kinase activity is required for interleukin-1 (IL-1) receptor- and toll-like receptor 7-mediated signaling and gene expression. *J. Biol. Chem. 282*, 13552−13560.

(14) Lye, E., Mirtsos, C., Suzuki, N., Suzuki, S., and Yeh, W. C. (2004) The role of interleukin 1 receptor-associated kinase-4 (IRAK-4) kinase activity in IRAK-4-mediated signaling. *J. Biol. Chem. 279*, 40653−40658.

(15) Motshwene, P. G., Moncrieffe, M. C., Grossmann, J. G., Kao, C., Ayaluru, M., Sandercock, A. M., Robinson, C. V., Latz, E., and Gay, N. J. (2009) An oligomeric signaling platform formed by the Toll-like receptor signal transducers MyD88 and IRAK-4. *J. Biol. Chem. 284*, 25404−25411.

(16) Lin, S. C., Lo, Y. C., and Wu, H. (2010) Helical assembly in the MyD88-IRAK4-IRAK2 complex in TLR/IL-1R signalling. *Nature 465*, 885−890.

(17) Goh, E. T., Arthur, J. S., Cheung, P. C., Akira, S., Toth, R., and Cohen, P. (2012) Identification of the protein kinases that activate the E3 ubiquitin ligase Pellino 1 in the innate immune system. *Biochem. J. 441*, 339−346.
(18) Dunne, A., Carpenter, S., Brikos, C., Gray, P., Strelow, A., Wesche, H., Morrice, N., and O'Neill, L. A. (2010) IRAK1 and IRAK4 promote phosphorylation, ubiquitination, and degradation of MyD88 adaptor-like (Mal). *J. Biol. Chem. 285*, 18276−18282.
(19) Kollewe, C., Mackensen, A. C., Neumann, D., Knop, J., Cao, P., Li, S., Wesche, H., and Martin, M. U. (2004) Sequential autophosphorylation steps in the interleukin-1 receptor-associated kinase-1 regulate its availability as an adapter in interleukin-1 signaling. *J. Biol. Chem. 279*, 5227−5236.
(20) Tun-Kyi, A., Finn, G., Greenwood, A., Nowak, M., Lee, T. H., Asara, J. M., Tsokos, G. C., Fitzgerald, K., Israel, E., Li, X., Exley, M., Nicholson, L. K., and Lu, K. P. (2011) Essential role for the prolyl isomerase Pin1 in Toll-like receptor signaling and type I interferon-mediated immunity. *Nat. Immunol. 12*, 733−741.
(21) Conze, D. B., Wu, C. J., Thomas, J. A., Landstrom, A., and Ashwell, J. D. (2008) Lys63-linked polyubiquitination of IRAK-1 is required for interleukin-1 receptor- and toll-like receptor-mediated NF-κB activation. *Mol. Cell. Biol. 28*, 3538−3547.
(22) Lin, C. C., Huoh, Y. S., Schmitz, K. R., Jensen, L. E., and Ferguson, K. M. (2008) Pellino proteins contain a cryptic FHA domain that mediates interaction with phosphorylated IRAK1. *Structure 16*, 1806−1816.
(23) Haghayeghi, A., Sarac, A., Czerniecki, S., Grosshans, J., and Schock, F. (2010) Pellino enhances innate immunity in *Drosophila*. *Mech. Dev. 127*, 301−307.
(24) Kim, J. H., Sung, K. S., Jung, S. M., Lee, Y. S., Kwon, J. Y., Choi, C. Y., and Park, S. H. (2011) Pellino-1, an adaptor protein of interleukin-1 receptor/toll-like receptor signaling, is sumoylated by Ubc9. *Mol. Cells 31*, 85−89.
(25) Gan, L., and Li, L. (2010) Interleukin-1 Receptor-Associated Kinase-1 (IRAK-1) functionally associates with PKCε and VASP in the regulation of macrophage migration. *Mol. Immunol. 47*, 1278−1282.
(26) Niebuhr, K., Ebel, F., Frank, R., Reinhard, M., Domann, E., Carl, U. D., Walter, U., Gertler, F. B., Wehland, J., and Chakraborty, T. (1997) A novel proline-rich motif present in ActA of *Listeria monocytogenes* and cytoskeletal proteins is the ligand for the EVH1 domain, a protein module present in the Ena/VASP family. *EMBO J. 16*, 5433−5444.
(27) Pistor, S., Chakraborty, T., Walter, U., and Wehland, J. (1995) The bacterial actin nucleator protein ActA of *Listeria monocytogenes* contains multiple binding sites for host microfilament proteins. *Curr. Biol. 5*, 517−525.
(28) Ball, L. J., Kuhne, R., Hoffmann, B., Hafner, A., Schmieder, P., Volkmer-Engert, R., Hof, M., Wahl, M., Schneider-Mergener, J., Walter, U., Oschkinat, H., and Jarchau, T. (2000) Dual epitope recognition by the VASP EVH1 domain modulates polyproline ligand specificity and binding affinity. *EMBO J. 19*, 4903−4914.
(29) Ball, L. J., Jarchau, T., Oschkinat, H., and Walter, U. (2002) EVH1 domains: Structure, function and interactions. *FEBS Lett. 513*, 45−52.
(30) Krause, M., Dent, E. W., Bear, J. E., Loureiro, J. J., and Gertler, F. B. (2003) Ena/VASP proteins: Regulators of the actin cytoskeleton and cell migration. *Annu. Rev. Cell Dev. Biol. 19*, 541−564.
(31) Haffner, C., Jarchau, T., Reinhard, M., Hoppe, J., Lohmann, S. M., and Walter, U. (1995) Molecular cloning, structural analysis and functional expression of the proline-rich focal adhesion and microfilament-associated protein VASP. *EMBO J. 14*, 19−27.
(32) Rottner, K., Behrendt, B., Small, J. V., and Wehland, J. (1999) VASP dynamics during lamellipodia protrusion. *Nat. Cell Biol. 1*, 321−322.
(33) Vasioukhin, V., Bauer, C., Yin, M., and Fuchs, E. (2000) Directed actin polymerization is the driving force for epithelial cell-cell adhesion. *Cell 100*, 209−219.
(34) Reinhard, M., Rudiger, M., Jockusch, B. M., and Walter, U. (1996) VASP interaction with vinculin: A recurring theme of interactions with proline-rich motifs. *FEBS Lett. 399*, 103−107.
(35) Gertler, F. B., Niebuhr, K., Reinhard, M., Wehland, J., and Soriano, P. (1996) Mena, a relative of VASP and *Drosophila* Enabled, is implicated in the control of microfilament dynamics. *Cell 87*, 227−239.
(36) Wehrle-Haller, B., and Imhof, B. A. (2003) Actin, microtubules and focal adhesion dynamics during cell migration. *Int. J. Biochem. Cell Biol. 35*, 39−50.
(37) Goh, K. L., Cai, L., Cepko, C. L., and Gertler, F. B. (2002) Ena/VASP proteins regulate cortical neuronal positioning. *Curr. Biol. 12*, 565−569.
(38) Bear, J. E., Loureiro, J. J., Libova, I., Fassler, R., Wehland, J., and Gertler, F. B. (2000) Negative regulation of fibroblast motility by Ena/VASP proteins. *Cell 101*, 717−728.
(39) Grevengoed, E. E., Loureiro, J. J., Jesse, T. L., and Peifer, M. (2001) Abelson kinase regulates epithelial morphogenesis in *Drosophila*. *J. Cell Biol. 155*, 1185−1198.
(40) Boeda, B., Briggs, D. C., Higgins, T., Garvalov, B. K., Fadden, A. J., McDonald, N. Q., and Way, M. (2007) Tes, a specific Mena interacting partner, breaks the rules for EVH1 binding. *Mol. Cell 28*, 1071−1082.
(41) Piotukh, K., Gu, W., Kofler, M., Labudde, D., Helms, V., and Freund, C. (2005) Cyclophilin A binds to linear peptide motifs containing a consensus that is present in many human proteins. *J. Biol. Chem. 280*, 23668−23674.
(42) Delaglio, F., Grzesiek, S., Vuister, G. W., Zhu, G., Pfeifer, J., and Bax, A. (1995) NMRPipe: A multidimensional spectral processing system based on UNIX pipes. *J. Biomol. NMR 6*, 277−293.
(43) Goddard, T. D., and Kneller, D. G. (2008) *Sparky 3*, University of California, San Francisco.
(44) Mori, S., Abeygunawardana, C., Johnson, M. O., and van Zijl, P. C. (1995) Improved sensitivity of HSQC spectra of exchanging protons at short interscan delays using a new fast HSQC (FHSQC) detection scheme that avoids water saturation. *J. Magn. Reson., Ser. B 108*, 94−98.
(45) De, S., Greenwood, A. I., Rogals, M. J., Kovrigin, E. L., Lu, K. P., and Nicholson, L. K. (2012) Complete thermodynamic and kinetic characterization of the isomer-specific interaction between Pin1-WW domain and the amyloid precursor protein cytoplasmic tail phosphorylated at Thr668. *Biochemistry 51*, 8583−8596.
(46) Kovrigin, E. L. (2012) NMR line shapes and multi-state binding equilibria. *J. Biomol. NMR 53*, 257−270.
(47) McConnell, H. M. (1958) Reaction rates by nuclear magnetic resonance. *J. Chem. Phys. 28*, 430−431.
(48) Palmer, A. G., III, Fairbrother, W. J., Cavanagh, J., Skelton, N. J., and Rance, M. (2007) *Protein NMR spectroscopy: Principles and practice*, 2nd ed., Academic Press, London.
(49) Prehoda, K. E., Lee, D. J., and Lim, W. A. (1999) Structure of the enabled/VASP homology 1 domain-peptide complex: A key component in the spatial control of actin assembly. *Cell 97*, 471−480.
(50) Guex, N., and Peitsch, M. C. (1997) SWISS-MODEL and the Swiss-PdbViewer: An environment for comparative protein modeling. *Electrophoresis 18*, 2714−2723.
(51) Farrow, N. A., Zhang, O., Forman-Kay, J. D., and Kay, L. E. (1994) A heteronuclear correlation experiment for simultaneous determination of ^{15}N longitudinal decay and chemical exchange rates of systems in slow equilibrium. *J. Biomol. NMR 4*, 727−734.
(52) Dawson, J. E., Seckute, J., De, S., Schueler, S. A., Oswald, A. B., and Nicholson, L. K. (2009) Elucidation of a pH-folding switch in the *Pseudomonas syringae* effector protein AvrPto. *Proc. Natl. Acad. Sci. U.S.A. 106*, 8543−8548.
(53) Hagerman, P. J., and Baldwin, R. L. (1976) A quantitative treatment of the kinetics of the folding transition of ribonuclease A. *Biochemistry 15*, 1462−1473.
(54) Ng, K. K., and Weis, W. I. (1998) Coupling of prolyl peptide bond isomerization and Ca^{2+} binding in a C-type mannose-binding protein. *Biochemistry 37*, 17977−17989.

(55) Reimer, U., Scherer, G., Drewello, M., Kruber, S., Schutkowski, M., and Fischer, G. (1998) Side-chain effects on peptidyl-prolyl cis/trans isomerisation. *J. Mol. Biol. 279*, 449−460.
(56) Fedorov, A. A., Fedorov, E., Gertler, F., and Almo, S. C. (1999) Structure of EVH1, a novel proline-rich ligand-binding module involved in cytoskeletal dynamics and neural function. *Nat. Struct. Biol. 6*, 661−665.
(57) Kay, B. K., Williamson, M. P., and Sudol, M. (2000) The importance of being proline: The interaction of proline-rich motifs in signaling proteins with their cognate domains. *FASEB J. 14*, 231−241.
(58) Schmidpeter, P. A., Jahreis, G., Geitner, A. J., and Schmid, F. X. (2011) Prolyl isomerases show low sequence specificity toward the residue following the proline. *Biochemistry 50*, 4796−4803.
(59) Zoldak, G., Aumuller, T., Lucke, C., Hritz, J., Oostenbrink, C., Fischer, G., and Schmid, F. X. (2009) A library of fluorescent peptides for exploring the substrate specificities of prolyl isomerases. *Biochemistry 48*, 10423−10436.
(60) Kloks, C. P., Tessari, M., Vuister, G. W., and Hilbers, C. W. (2004) Cold shock domain of the human Y-box protein YB-1. Backbone dynamics and equilibrium between the native state and a partially unfolded state. *Biochemistry 43*, 10237−10246.
(61) Thies, M. J., Mayer, J., Augustine, J. G., Frederick, C. A., Lilie, H., and Buchner, J. (1999) Folding and association of the antibody domain CH3: Prolyl isomerization preceeds dimerization. *J. Mol. Biol. 293*, 67−79.
(62) Connors, K. A. (1990) *Chemical Kinetics*, VCH, New York.
(63) Volkman, B. F., Prehoda, K. E., Scott, J. A., Peterson, F. C., and Lim, W. A. (2002) Structure of the N-WASP EVH1 domain-WIP complex: Insight into the molecular basis of Wiskott-Aldrich syndrome. *Cell 111*, 565−576.
(64) Bachmann, C., Fischer, L., Walter, U., and Reinhard, M. (1999) The EVH2 domain of the vasodilator-stimulated phosphoprotein mediates tetramerization, F-actin binding, and actin bundle formation. *J. Biol. Chem. 274*, 23549−23557.
(65) Roitt, I. M., Brostoff, J., and Male, D. K. (2001) *Immunology*, 6th ed., Mosby, New York.
(66) Watters, T. M., Kenny, E. F., and O'Neill, L. A. (2007) Structure, function and regulation of the Toll/IL-1 receptor adaptor proteins. *Immunol. Cell Biol. 85*, 411−419.
(67) Qin, J., Qian, Y., Yao, J., Grace, C., and Li, X. (2005) SIGIRR inhibits interleukin-1 receptor- and toll-like receptor 4-mediated signaling through different mechanisms. *J. Biol. Chem. 280*, 25233−25241.
(68) Weiss, A., and Schlessinger, J. (1998) Switching signals on or off by receptor dimerization. *Cell 94*, 277−280.
(69) Lemmon, M. A., and Schlessinger, J. (1994) Regulation of signal transduction and signal diversity by receptor oligomerization. *Trends Biochem. Sci. 19*, 459−463.
(70) Wilson, N. S., Dixit, V., and Ashkenazi, A. (2009) Death receptor signal transducers: Nodes of coordination in immune signaling networks. *Nat. Immunol. 10*, 348−355.
(71) McCulloch, C. A., Downey, G. P., and El-Gabalawy, H. (2006) Signalling platforms that modulate the inflammatory response: New targets for drug development. *Nat. Rev. Drug Discovery 5*, 864−876.
(72) Sun, L., Deng, L., Ea, C. K., Xia, Z. P., and Chen, Z. J. (2004) The TRAF6 ubiquitin ligase and TAK1 kinase mediate IKK activation by BCL10 and MALT1 in T lymphocytes. *Mol. Cell 14*, 289−301.
(73) Dong, W., Liu, Y., Peng, J., Chen, L., Zou, T., Xiao, H., Liu, Z., Li, W., Bu, Y., and Qi, Y. (2006) The IRAK-1-BCL10-MALT1-TRAF6-TAK1 cascade mediates signaling to NF-κB from Toll-like receptor 4. *J. Biol. Chem. 281*, 26029−26040.
(74) Wedemeyer, W. J., Welker, E., and Scheraga, H. A. (2002) Proline cis-trans isomerization and protein folding. *Biochemistry 41*, 14637−14644.
(75) Gothel, S. F., and Marahiel, M. A. (1999) Peptidyl-prolyl cis-trans isomerases, a superfamily of ubiquitous folding catalysts. *Cell. Mol. Life Sci. 55*, 423−436.
(76) Colgan, J., Asmal, M., Neagu, M., Yu, B., Schneidkraut, J., Lee, Y., Sokolskaja, E., Andreotti, A., and Luban, J. (2004) Cyclophilin A regulates TCR signal strength in CD4+ T cells via a proline-directed conformational switch in Itk. *Immunity 21*, 189−201.
(77) Sarkar, P., Saleh, T., Tzeng, S. R., Birge, R. B., and Kalodimos, C. G. (2011) Structural basis for regulation of the Crk signaling protein by a proline switch. *Nat. Chem. Biol. 7*, 51−57.
(78) Bannon, J. H., O'Donovan, D. S., Kennelly, S. M., and Mc Gee, M. M. (2012) The peptidyl prolyl isomerase cyclophilin A localizes at the centrosome and the midbody and is required for cytokinesis. *Cell Cycle 11*, 1340−1353.
(79) Akimoto, M., Selvaratnam, R., McNicholl, E. T., Verma, G., Taylor, S. S., and Melacini, G. (2013) Signaling through dynamic linkers as revealed by PKA. *Proc. Natl. Acad. Sci. U.S.A. 110*, 14231−14236.
(80) Vallee-Belisle, A., Ricci, F., and Plaxco, K. W. (2009) Thermodynamic basis for the optimization of binding-induced biomolecular switches and structure-switching biosensors. *Proc. Natl. Acad. Sci. U.S.A. 106*, 13802−13807.
(81) Mallis, R. J., Brazin, K. N., Fulton, D. B., and Andreotti, A. H. (2002) Structural characterization of a proline-driven conformational switch within the Itk SH2 domain. *Nat. Struct. Biol. 9*, 900−905.
(82) Krause, M., Sechi, A. S., Konradt, M., Monner, D., Gertler, F. B., and Wehland, J. (2000) Fyn-binding protein (Fyb)/SLP-76-associated protein (SLAP), Ena/vasodilator-stimulated phosphoprotein (VASP) proteins and the Arp2/3 complex link T cell receptor (TCR) signaling to the actin cytoskeleton. *J. Cell Biol. 149*, 181−194.
(83) May, R. C., and Machesky, L. M. (2001) Phagocytosis and the actin cytoskeleton. *J. Cell Sci. 114*, 1061−1077.
(84) Coppolino, M. G., Krause, M., Hagendorff, P., Monner, D. A., Trimble, W., Grinstein, S., Wehland, J., and Sechi, A. S. (2001) Evidence for a molecular complex consisting of Fyb/SLAP, SLP-76, Nck, VASP and WASP that links the actin cytoskeleton to Fcγ receptor signalling during phagocytosis. *J. Cell Sci. 114*, 4307−4318.
(85) Maa, M.-C., and Leu, T.-H. (2011) Activation of Toll-like receptors induces macrophage migration via the iNOS/Src/FAK pathway. *BioMedicine 1*, 11−15.
(86) Chen, Y. J., Hsieh, M. Y., Chang, M. Y., Chen, H. C., Jan, M. S., Maa, M. C., and Leu, T. H. (2012) Eps8 protein facilitates phagocytosis by increasing TLR4-MyD88 protein interaction in lipopolysaccharide-stimulated macrophages. *J. Biol. Chem. 287*, 18806−18819.
(87) Creamer, H. R., Hunter, N., Bullock, W. W., and Gabler, W. L. (1991) Concurrent lipopolysaccharide enhances chemotactic response of human polymorphonuclear leukocytes to bacterial chemotaxin. *Inflammation 15*, 201−211.
(88) Yi, L., Chandrasekaran, P., and Venkatesan, S. (2012) TLR signaling paralyzes monocyte chemotaxis through synergized effects of p38 MAPK and global Rap-1 activation. *PLoS One 7*, e30404.
(89) McTaggart, S. J., Obbard, D. J., Conlon, C., and Little, T. J. (2012) Immune genes undergo more adaptive evolution than non-immune system genes in *Daphnia pulex*. *BMC Evol. Biol. 12*, 63.
(90) Reinhard, M., Jouvenal, K., Tripier, D., and Walter, U. (1995) Identification, purification, and characterization of a zyxin-related protein that binds the focal adhesion and microfilament protein VASP (vasodilator-stimulated phosphoprotein). *Proc. Natl. Acad. Sci. U.S.A. 92*, 7956−7960.
(91) Krause, M., Leslie, J. D., Stewart, M., Lafuente, E. M., Valderrama, F., Jagannathan, R., Strasser, G. A., Rubinson, D. A., Liu, H., Way, M., Yaffe, M. B., Boussiotis, V. A., and Gertler, F. B. (2004) Lamellipodin, an Ena/VASP ligand, is implicated in the regulation of lamellipodial dynamics. *Dev. Cell 7*, 571−583.
(92) Domann, E., Wehland, J., Rohde, M., Pistor, S., Hartl, M., Goebel, W., Leimeister-Wachter, M., Wuenscher, M., and Chakraborty, T. (1992) A novel bacterial virulence gene in *Listeria monocytogenes* required for host cell microfilament interaction with homology to the proline-rich region of vinculin. *EMBO J. 11*, 1981−1990.
(93) DeLano, W. L. (2002) *The PyMOL Molecular Graphics System*, version 1.3, Schrödinger, LLC, Portland, OR.